Solar Energy Materials & Solar Cells 234 (2022) 111428

Contents lists available at ScienceDirect

Solar Energy Materials and Solar Cells

journal homepage: www.elsevier.com/locate/solmat

On the quantification of Auger recombination in crystalline silicon

Lachlan E. Black *, Daniel H. Macdonald

School of Engineering, Building 31, The Australian National University, Canberra, 2600, ACT, Australia

ARTICLE INFO

Keywords:
Crystalline silicon
Auger recombination
Carrier lifetime
Photoconductance measurements

ABSTRACT

Quantification of Auger recombination in crystalline silicon is usually challenging because it requires distinguishing Auger recombination from extrinsic recombination processes, especially at the surface. In this work we exploit the known injection dependence of surface recombination at surfaces passivated by highly charged dielectric films to assess the value of the ambipolar Auger coefficient C_{amb} in crystalline silicon from carefully calibrated photoconductance decay measurements of high-lifetime Si wafers. A value of $C_{amb} = (2.11 \pm 0.02) \times 10^{-30}\ \mathrm{cm^6\ s^{-1}}$ is determined for both *n*- and *p*-type Si, independent of the dopant concentration for moderately doped samples near 300 K. Furthermore, by exploiting the expected equality of the surface saturation current density J_{0s} for identically processed *n*- and *p*-type substrates, we are able to estimate the relative contributions of *ehh* and *eeh* Auger processes to C_{amb} under the same doping and injection regime. The resulting ratio $C_n/C_p = 2.81$ is in close agreement with the value of 2.91 derived from the data of Dziewior and Schmid at high dopant concentrations, which we reassess in light of modern mobility models. Based on our own data and literature data at higher concentrations, we offer a revised parameterisation of the Auger recombination rate in c-Si as a function of dopant concentration and injection level which is consistent with these findings. This revised parameterisation is also shown to be consistent with the most recent record lifetimes reported by other authors. Finally, we suggest experimental considerations relevant for future efforts to further refine the Auger parameterisation.

1. Introduction

Auger recombination, in which a recombining electron–hole pair give up their excess energy to a third carrier (either an electron or a hole), is an intrinsic and therefore unavoidable process in semiconductors. Auger recombination processes are particularly important in indirect-bandgap semiconductors, where radiative recombination is weak. In particular, they dominate bulk recombination in intrinsic or moderately doped high-purity crystalline silicon (c-Si) under 1-Sun illumination, and in highly doped material under all conditions, and effectively limit the ultimate achievable energy conversion efficiency of c-Si solar cells [1,2].

Despite its importance in c-Si devices, quantifying Auger recombination is challenging because, unlike radiative recombination, Auger recombination cannot be measured directly, and its contribution must therefore be separated from the total measured recombination, which also includes contributions from intrinsic radiative recombination and extrinsic recombination due to defects in the silicon bulk and at the surfaces. Consequently the Auger coefficients are most easily determined under low-injection conditions in very highly doped material ($> 1 \times 10^{18}\ \mathrm{cm^{-3}}$), where the contribution of other recombination mechanisms is negligible. However, it has long been known that the Auger coefficients determined at such high doping levels significantly underestimate the Auger recombination rate at lower carrier concentrations, because of the influence of Coulomb enhancement [3,4].

Attempts to quantify Auger recombination in c-Si at low-to-intermediate carrier concentrations must therefore deal with the issue of how to separate it from other recombination components. The radiative recombination coefficient can be determined independently via the generalised Planck equation [5,6], and current values are widely accepted [7–10], Meanwhile, extrinsic bulk recombination can be made very small in high-quality float-zone (FZ) material. This leaves surface recombination as the major source of error in determinations of the Auger recombination rate from total measured recombination.

Previous efforts to quantify Auger recombination in c-Si at lower carrier concentrations have generally either sought to quantify and eliminate the surface recombination component (for example by experiments in which the substrate thickness is systematically varied and the bulk lifetime taken from the extrapolation to infinite thickness) [11–13], or have sought to minimise surface recombination by means of the best available surface passivation techniques, and have subsequently assumed remaining recombination to be due to intrinsic processes [1,

* Corresponding author.
E-mail address: lachlan.black@anu.edu.au (L.E. Black).

https://doi.org/10.1016/j.solmat.2021.111428
Received 10 August 2021; Received in revised form 29 September 2021; Accepted 1 October 2021
Available online 19 October 2021

2,4,14], The latter approach was adopted by the currently most widely accepted description of Auger recombination in c-Si, that of Richter et al. [1], which updated the methodologically similar work of Kerr and Cuevas [2].

This approach has the advantage that potential complexities in the physics do not need to be dealt with directly but are simply treated empirically. However, it also has the drawback that the determined recombination rates which are attributed to Auger processes are dependent on technologically achievable levels of bulk material quality and surface passivation. As these improve, so the Auger coefficients need to be continually reassessed and updated. Thus, such approaches can only ever determine a lower limit for the intrinsic lifetime.

Indeed, the limitations of the parameterisation of Richter et al. have already been apparent for some time. In particular, multiple authors have now reported measured carrier lifetimes for *n*-type Si that significantly exceed those predicted by this parameterisation [15–21]. More recently, measurements of lifetimes exceeding the parameterisation in *p*-type Si have also been reported [18]. These higher lifetimes have been enabled by continued improvements in surface passivation quality, including the availability of new passivation materials and techniques, the use of thicker substrates, as well as a focus on minimising lateral recombination channels resulting from spatial non-uniformities and edge recombination [19,22] (the latter in particular likely limited the lifetimes of the Al_2O_3-passivated *n*-type samples of Richter et al.). At the same time, the work of Grant et al. [23,24] and Niewelt et al. [18] has made clear that extrinsic bulk defects continue to significantly limit bulk lifetimes even in supposedly ultra-pure FZ Si material, and significant bulk lifetime improvements have been obtained through the use of advanced gettering and annealing treatments designed to minimise the concentration of these remaining defects. A partially updated Auger parameterisation for *n*-type Si has been offered by Veith-Wolf et al. [19] on the basis of their latest data. A more comprehensive revision is currently in preparation by Niewelt et al. [25]. We will discuss the relationship between this latter work and our own results in more detail at the end of the paper.

Besides underestimation of the low-injection Auger lifetime, another unsatisfactory aspect of most recent parameterisations (including those of Kerr et al., Richter et al., and Veith-Wolf et al.) is their different treatment of Auger recombination depending on whether charge carriers originate from doping or excess-carrier injection. Since, in principle, electrons and holes generated by equilibrium and non-equilibrium processes are indistinguishable, this is physically inconsistent. There is also disagreement between these parameterisations and the model of Sinton and Swanson for Auger recombination in highly injected Si [26], which remains widely used in analysis of lifetime data to extract the surface saturation current density J_{0s} via the method of Kane and Swanson [27]. For well-passivated samples, the choice of which of these models to use has a significant impact on the value of J_{0s} extracted in this way, and it is not clear which, if any, is to be trusted. Although widely employed, the model of Sinton and Swanson was published over three decades ago, and has not been updated in light of subsequent changes to commonly accepted values of the relevant material constants.

In the present work, we propose a novel approach for determining the Auger coefficients, and use it to assess their values in c-Si. As in most recent studies, we base our analysis on photoconductance decay measurements of the excess carrier lifetime in well-passivated, high-quality FZ c-Si wafers. Here we take advantage of recent improvements which we have demonstrated in the accuracy of these measurements, which are achieved by properly accounting for the dependence of the calibration factors on sample thickness owing to the decay of the magnetic field with distance from the inductive coil [28]. Additionally, rather than basing our model on the maximum measured lifetimes in low injection, we exploit the distinct injection dependences of the different recombination processes in order to allow extraction of the ambipolar Auger component (in this respect our approach is similar to that of Sinton and Swanson [26]).

However, the chief novelty of our approach is based in our treatment of surface recombination. In particular, we make use of the known injection dependence of surface recombination at strongly accumulated or inverted surfaces, in situations where it can be described by an injection-independent surface saturation current density J_{0s}. Furthermore, we subsequently exploit the independence of J_{0s} with respect to doping, and its equality across identically processed samples, in order to permit an estimation of the ratio between the low-injection Auger coefficients for *n*- and *p*-type c-Si. This allows the construction of a complete, self-consistent model of Auger recombination in the examined doping and injection range, which we extend to higher doping ranges using data from the literature. In this way we aim to obtain an estimate not merely of a lower limit to the intrinsic lifetime, but of the true intrinsic lifetime. We show that a unified description of Auger recombination, in which free carriers resulting from doping and injection are treated on an equal footing, without unexplained fractional exponents, and with close symmetry between the screening functions for electrons and holes, is both feasible and consistent with the available data. Along the way, we outline a number of experimental considerations relevant for future efforts to improve the accuracy of the Auger parameterisation, and suggest future research directions.

2. Theory

The total volumetric recombination rate of excess carriers U_{total} is given by the sum of the recombination rates due to the individual processes

$$U_{total} = U_{Auger} + U_{rad} + U_{SRH} + U_s(A/V) \tag{1}$$

where U_{Auger}, U_{rad}, U_{SRH}, and U_s are the net recombination rates due to Auger recombination, radiative recombination, bulk Shockley–Read–Hall (SRH) recombination, and surface recombination respectively, A is the surface area and V the volume of the sample.

The Auger recombination rate U_{Auger} is given by

$$U_{Auger} = C_p(p^2n - p_0^2n_0) + C_n(pn^2 - p_0n_0^2) \tag{2}$$

where C_p and C_n are the Auger coefficients for the electron–hole–hole (*ehh*) and electron–electron–hole (*eeh*) processes respectively, p and n are the concentrations of holes and electrons, and p_0 and n_0 are these same concentrations in equilibrium. Under high-injection conditions ($p \approx n \gg p_0, n_0$),

$$\begin{aligned} U_{Auger,hi} &= C_npn^2 + C_pp^2n \\ &= (C_n + C_p)\Delta n^3 = C_{amb}\Delta n^3 \end{aligned} \tag{3}$$

where $C_{amb} = C_n + C_p$ is called the ambipolar Auger coefficient, and $\Delta n = n - n_0 = p - p_0$ is the excess carrier concentration.

The net radiative recombination rate U_{rad} is given by

$$U_{rad} = (1 - f_{reabs,bb})B_{rad}(pn - p_0n_0) \tag{4}$$

where B_{rad} is the radiative coefficient ($4.76 \times 10^{15}\,cm^3\,s^{-1}$ at 300 K in silicon at low carrier concentrations [10]) and $f_{reabs,bb}$ is the fraction of radiatively emitted photons reabsorbed via band-to-band processes (photon recycling) [29].

In general, the surface recombination rate U_s is a complex function of p and n that depends on the surface band bending and the capture cross-sections and energy distribution of the interface states. However, as demonstrated by [30], in the limiting case of dielectric-passivated surfaces in strong accumulation or inversion, the surface recombination rate U_s may be written as

$$U_s = \frac{J_{0s}}{qn_i^2}(pn - p_0n_0) \tag{5}$$

where J_{0s} is the surface saturation current density, q is the fundamental electron charge, $n_i = (p_0n_0)^{1/2}$ is the intrinsic carrier concentration, and

J_{0s}/n_i^2 is (under these limiting conditions) independent of the doping and excess carrier concentration. This situation holds for most light-to-moderately doped silicon surfaces passivated by a dielectric with a large fixed charge, such as Al_2O_3 or SiN_x. In particular we shall show later that it holds for the samples which we consider in this work.

Per definition, the effective excess carrier lifetime τ_{eff} is related to U_{total} by

$$U_{total} \equiv \tau_{eff}^{-1} \Delta n \tag{6}$$

where Δn is the excess carrier concentration. Combining Eqs. (1)–(2), (4)–(6) we can write, for conditions far from equilibrium ($pn \gg p_0 n_0$),

$$\tau_{eff}^{-1}\Delta n = C_p ppn + C_n pnn + \tau_{SRH}^{-1}\Delta n + (1 - f_{reabs,bb})B_{rad}pn + \frac{2}{W}\frac{J_{0s}}{qn_i^2}pn \tag{7}$$

where for the surface recombination component we have assumed a symmetrical wafer geometry with thickness W. Here we also implicitly assume that the carrier concentrations are approximately uniform throughout the sample. We shall later demonstrate this to be true for our samples.

Rearranging terms, and expressing p and n in terms of Δn, this can be rewritten as

$$(\tau_{eff}^{-1} - \tau_{SRH}^{-1})(p_0 + n_0 + \Delta n)^{-1} = C_p p_0 + C_n n_0 + (C_p + C_n)\Delta n + (1 - f_{reabs,bb})B_{rad} + \frac{2}{W}\frac{J_{0s}}{qn_i^2} \tag{8}$$

Thus, when τ_{SRH}^{-1} is negligible, and in cases when J_{0s}/n_i^2 can be assumed independent of Δn, a plot of $\tau_{eff}^{-1}(p_0+n_0+\Delta n)^{-1}$ vs Δn should yield a linear function with a slope equal to $C_{amb} = C_p + C_n$, and an intercept at $\Delta n = 0$ given by $(1 - f_{reabs,bb})B_{rad} + C_p p_0 + C_n n_0 + 2J_{0s}(qn_i^2 W)^{-1}$.

We have until this point treated B_{rad}, C_p, and C_n as constants that are independent of dopant and carrier concentrations. In reality this is not the case. Both the radiative and Auger coefficients are known to decrease at high dopant and carrier concentrations, which has been attributed to screening of Coulomb-enhancement effects present at low carrier densities [3,4,8,31,32]. Consequently these coefficients should more generally be written as

$$B_{rad} = g_{eh} B_{rad,0} \tag{9}$$

$$C_p = g_{ehh} C_{p0} \tag{10}$$

$$C_n = g_{eeh} C_{n0} \tag{11}$$

where g_{eh}, g_{ehh}, and g_{eeh} are enhancement factors which depend on the excess carrier and dopant concentrations, and $B_{rad,0}$, C_{p0} and C_{n0} are the values of these parameters in the free-particle limit at high concentrations. Additionally, strictly it is not J_{0s}/n_i^2 that is independent of carrier concentration in (5), but rather $J_{0s}/n_{i,s}^2$, where $n_{i,s}$ is the value of the intrinsic carrier concentration at the surface [30]. This makes J_{0s}/n_i^2 proportional to $n_{i,s}^2/n_i^2$, which in principle is injection-dependent due to non-uniform bandgap narrowing between the surface and the quasi-neutral region at higher carrier concentrations. We will consider the uncertainties created by these dependencies later, however for now we note that in the carrier density range which we examine they represent essentially second-order effects. They will become important mainly when we come to consider the dependence of C_p and C_n on dopant density.

3. Experimental

3.1. Sample preparation

Symmetrically passivated lifetime test structures were fabricated on RCA (Radio Corporation of America)-cleaned, 4 inch diameter, planar (100) FZ c-Si wafers. These samples were initially processed and characterised as part of unrelated experiments in two separate laboratories.

Table 1
Details of samples investigated in this work.

Sample	Type	p_0/n_0 (cm^{-3})	W (μm)	Max. τ_{eff} (ms)	Passivation
#1	n	9.43×10^{13}	317	111	PO_x/Al_2O_3
#2	n	2.81×10^{15}	289	13.9	Al_2O_3
#3	p	5.04×10^{15}	285	7.36	Al_2O_3
#4	n	6.88×10^{16}	251	0.121	SiO_2

Sample #1 was a chemically polished ~50 Ω cm n-type wafer (317 μm thick). This received a Tabula Rasa annealing treatment at 1000 °C in O_2 to annihilate possible nitrogen vacancies [23,24], followed by an hydrofluoric (HF) acid etch to remove the grown SiO_2 prior to RCA cleaning (with a final HF etch to remove the RCA oxide immediately prior to passivation). PO_x/Al_2O_3 passivation stacks [33–36] (4.5 nm/11 nm thick) were deposited in an Oxford Instruments FlexAL atomic layer deposition (ALD) reactor at 100 °C from trimethylphosphate, trimethylaluminium (TMA), and O_2 plasma. Following PO_x/Al_2O_3 deposition, the sample was annealed at 400 °C in N_2 for 10 min in a tube furnace to activate the passivation.

Samples #2 and #3 were double-side-polished n- and p-type wafers (Topsil) with a thickness of ~290 μm and a nominal resistivity of 1–5 Ωcm. The wafers were cleaved in half prior to processing in order to allow the p- and n-type samples to be processed in parallel. Al_2O_3 surface-passivation layers were deposited on both sides of the wafers by plasma-assisted ALD in the same Oxford Instruments FlexAL reactor. The chemical oxide was removed by immersion in 1 % HF solution for 1 min immediately prior to Al_2O_3 deposition. ~15 nm thick Al_2O_3 films were deposited at 25 °C using 110 cycles of trimethylaluminium (TMA) and O_2 plasma (200 W, 15 mTorr, 10 s). We note that although passivation by Al_2O_3 deposited by plasma ALD at such low temperatures has previously been reported to be relatively poor [37], we have recently obtained passivation with such films comparable to that of those deposited at higher temperature, when using a longer oxygen plasma step. Following film deposition, the samples were annealed in a Jipelec rapid thermal processing system at a series of increasing temperatures from 200 up to 500 °C in steps of 50 °C in N_2 ambient for 10 min at a time. The highest lifetime was obtained after annealing at 400 °C and we shall only discuss this data in this work.

Key properties of the samples investigated in this work are summarised in Table 1.

For Sample #1, the effective excess carrier lifetime was measured as a function of excess carrier concentration using a Sinton Instruments WCT-120 inductively coupled photoconductance lifetime tester. The temperature of the sample during the measurement was measured to be (303.5 ± 0.1) K using a thermocouple attached to the sample stage (the stage is heated slightly above room temperature by an uncontrolled, fixed-setting heater). The sample was left on the stage for some time prior to the measurement to allow equilibration of its temperature with the stage. For Samples 2 and 3, lifetime was measured in a similar way using a Sinton Instruments WCT-120TS lifetime tester. In this case lifetime measurements were performed at room temperature ((21 ± 1) °C as measured by a thermocouple built into the measurement stage).

Both lifetime measurement systems were carefully calibrated using specially prepared calibration sample sets, taking into account the dependence of the coil sensitivity on wafer thickness, as described in detail in [28]. These systems are those described as WCT-120 #1 and WCT-120TS #1 in the preceding work. Measurements were performed under both transient and quasi-steady-state (QSS) excitation conditions, corresponding to the 1/64 and 1/1 power modes of the flash. The former produces a short, sharply decaying excitation profile which allows measurements under true transient conditions (zero generation rate),

while the latter produces a more slowly decaying (~2 ms time constant) excitation with a higher peak intensity, which allows measurements at higher carrier concentrations.

Wafer thickness was measured using a contact dial-gauge system with digital readout and 1 μm resolution. The average thickness was determined from measurements at multiple points (at least 5) on each wafer in the vicinity of the region measured by the photoconductance coil. For the double-side-polished lifetime samples, lateral thickness variation was smaller than the resolution of the measurement.

The resistivity of all wafers was measured by the same calibrated WCT-120 photoconductance system used to perform the lifetime measurements of Sample #1. Measurements were performed in the dark as part of a standard system calibration procedure together with a full calibration wafer set. Multiple measurements of each wafer were made to identify and eliminate potential outlier readings. Temperature was monitored using a thermocouple attached to the sample stage. The dopant density was calculated from the measured resistivity using the temperature-dependent mobility model of Klaassen [38,39]. As an additional check, wafer resistivity was also measured by the four-point-probe method in the manner described in [28]. Dopant concentrations determined by this method were confirmed to closely match those determined from the dark conductance measured by the coil, after temperature correction.

3.2. Determination of $\tau_{eff}(\Delta n)$

In order to determine the carrier lifetime from the measured photoconductance decay, we first need to determine $\Delta n(t)$ from the time-dependent conductance. When the concentrations of electrons and holes n and p are spatially uniform, the total conductance σ is simply given by

$$\sigma = qW(\mu_p p + \mu_n n) \tag{12}$$

where W is the wafer thickness, and μ_p and μ_n are the hole and electron mobilities. Substituting $n = n_0 + \Delta n$ and $p = p_0 + \Delta n$, and rewriting in terms of Δn, we have

$$\Delta n = \frac{\sigma q^{-1} W^{-1} - \mu_p p_0 - \mu_n n_0}{\mu_p + \mu_n} \tag{13}$$

In conventional analyses of c-Si photoconductance decay measurements it is usually tacitly assumed that $\mu_p p_0 + \mu_n n_0$ is independent of Δn, so that only the excess conductance $\Delta\sigma = \sigma - \sigma_0$ need be considered. However, both μ_p and μ_n decrease with increasing carrier concentration, so that this approach systematically underestimates Δn. By calculating Δn from (13) we take account of the fact that the conductivity contribution of the equilibrium carriers is also a function of the excess carrier concentration.

The most commonly used mobility model for c-Si photoconductance analysis is that employed in the Sinton lifetime measurement software and described in [13], which is an empirical parameterisation of the measurements of Dannhäuser and Krausse [40,41] of the carrier mobility sum $\mu_p + \mu_n$ in lowly-doped, highly injected silicon at room temperature. However, this model does not account for the temperature-dependence of mobility, which is significant even for deviations of several degrees around room temperature. Nor does it provide the dependence of μ_p and μ_n on Δn individually, as required by (13). Therefore we choose instead to calculate μ_p and μ_n using the unified, physically-based model of Klaassen [38,39] (with the amendments included in the implementations of Sentaurus and PV Lighthouse[1]),

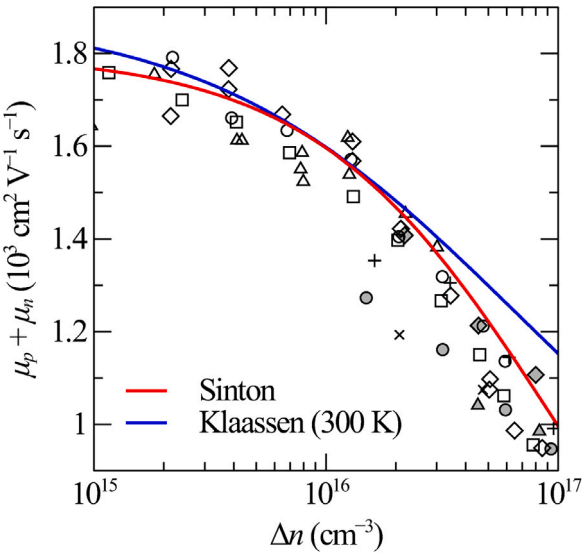

Fig. 1. Carrier mobility sum $\mu_p + \mu_n$ vs excess carrier concentration Δn in intrinsic c-Si, as measured by Dannhäuser [40] (open symbols) and Krausse [41] (filled symbols) at room temperature. Lines show the empirical parameterisation of the same data used in the Sinton measurement software [13], as well as the physically-based model of Klaassen [38,39] at 300 K.

which accounts separately for the influence of carrier concentration, doping, and temperature, and is the most widely accepted general model for mobility in c-Si.

Klaassen's model predicts a higher mobility sum at higher carrier concentrations than measured by Dannhäuser and Krausse, or given by the Sinton parameterisation, which Klaassen suggested could be due to sample heating in the experiments of Dannhäuser and Krausse. However, over the injection range of 5×10^{15} cm^{-3} to 1.5×10^{16} cm^{-3}, the model of Klaassen at 300 K is in excellent agreement with the Sinton parameterisation, and falls within the scatter of the experimental data, as shown in Fig. 1. Therefore, extraction of C_{amb} in this range introduces the least uncertainty based on the choice of mobility model. In the low-injection limit, the model of Klaassen coincides exactly with the widely accepted parameterisation of Thurber et al. [42,43] for the equilibrium mobility at 300 K, and should therefore be more accurate than the Sinton parameterisation.

The effective carrier lifetime τ_{eff} was calculated from $\Delta n(t)$ according to [44]

$$\tau_{eff} = \frac{\Delta n}{G(t) - (\mathrm{d}\Delta n/\mathrm{d}t)} \tag{14}$$

where $G(t)$ is the time-dependent average volumetric generation rate due to optical excitation, expressed in units of inverse volume and time, which is calculated according to

$$G(t) = C_{opt}\Phi(t)W^{-1} \tag{15}$$

where $\Phi(t)$ is the time-dependent incident photon flux measured by the lifetime tester system using a calibrated reference cell, and C_{opt} is a sample-dependent optical constant accounting for the fraction of incident photons absorbed by the sample as well as spectral mismatch between the excitation source and the calibration spectrum of the reference cell [45]. Note that $G(t)$ was assumed equal to zero for measurements performed in the transient regime.

The value of C_{opt} was determined by adjusting this value to give agreement between measurements of $\tau_{eff}(\Delta n)$ performed under "transient" and "QSS" excitation conditions in the overlapping injection range. As explained by [46], this is equivalent to assuming self-consistency between the applied mobility model and the mobility sum values implied by the photoconductance data.

[1] These implementations include the following amendments to Klaassen's published model [38]: (i) r_5 in Table 2 is set to 0.8552 rather than −0.01552, and (ii) Eq. A3 is modified such that P_{CWe} is determined with $N_{e,sc}$ rather than $(Z_D^3 N_I)$, and P_{CWh} is determined with $N_{h,sc}$ rather than $(Z_A^3 N_I)$. These changes result in a better fit to Klaassen's own published model outputs (in particular the solid calculated lines in Figs. 6 and 7 of [38]), which in turn agree better with the experimental data.

The choice of numerical procedure used to differentiate $\Delta n(t)$ in (14) is another important consideration, particularly during the early part of the photoconductance decay under "transient" excitation, when the decay is relatively rapid. We choose to perform the differentiation on $\ln(\Delta n)$ rather than Δn, since this results in a smaller curvature. At carrier concentrations above $2\times10^{15}\,\mathrm{cm^{-2}}$ we calculate the derivative using a 5-point cubic Savitzky–Golay convolution [47], in order to more accurately capture the rapid variation in slope during the initial part of the decay, while for $1\times10^{14}\,\mathrm{cm^{-3}} \le \Delta n \le 2\times10^{15}\,\mathrm{cm^{-3}}$ we apply a 5-point quadratic convolution, and for $\Delta n \le 1\times10^{14}\,\mathrm{cm^{-3}}$ a 9-point quadratic convolution, in order to reduce noise.

4. Results

4.1. Determination of the ambipolar Auger coefficient

Figs. 2a–c show τ_{eff} vs Δn determined for the high-resistivity n-type, and low-resistivity n- and p-type samples. We also plot the intrinsic lifetime according to Richter et al. [1] and Veith-Wolf et al. [19]. It can be seen that the measured lifetimes, though all excellent, do not exceed the parameterisation of Richter et al., although they all approach it closely at higher injection levels (the maximum measured lifetime values are nevertheless similar or higher than those actually measured by Richter et al. at similar dopant concentrations). However, a key feature of the proposed approach is that it does not require samples with lifetimes very closely approaching the intrinsic limit. Notably, none of the samples show a pronounced reduction in lifetime at low injection levels that would indicate significant bulk SRH or edge recombination.

Figs. 2d–f plot the corresponding values of $\tau_{eff}^{-1}(p_0+n_0+\Delta n)^{-1}$ vs Δn. It is immediately apparent that in all cases the data closely follows the linear trend predicted by Eq. (8), at least at lower carrier concentrations ($\Delta n \le 2\times10^{16}\,\mathrm{cm^{-3}}$) where there is less uncertainty in the mobility. This provides support for the underlying assumptions on which these expressions were based. We choose to fit the data in the range of $5\times10^{15}\,\mathrm{cm^{-3}} \le \Delta n \le 1.5\times10^{16}\,\mathrm{cm^{-3}}$, partly because of the good agreement of the different mobility models in this range, as discussed above, and also because the lower limit of $5\times10^{15}\,\mathrm{cm^{-3}}$ approximately corresponds to the point above which Auger recombination accounts for a majority of recombination in these samples, which helps to reduce sensitivity to other recombination channels. By fitting the slope of the data in this range, we derive initial estimates for the ambipolar Auger coefficient $C_{amb} = C_p + C_n$ of $1.94\times10^{-30}\,\mathrm{cm^6\,s^{-1}}$ for the high-resistivity n-type Sample #1, $1.96\times10^{-30}\,\mathrm{cm^6\,s^{-1}}$ for the low-resistivity n-type Sample #2, and $1.95\times10^{-30}\,\mathrm{cm^6\,s^{-1}}$ for the low-resistivity p-type Sample #3. The excellent agreement between these values is remarkable, given the differences in doping, sample preparation, measurement systems, and measurement temperatures involved.

4.2. Separation of C_p and C_n

Having determined a value for the ambipolar Auger coefficient $C_{amb} = C_p + C_n$, we would like now to separate the contributions of C_p and C_n. These terms appear in the expression for the intercept of $\tau_{eff}^{-1}(p_0+n_0+\Delta n)^{-1}$ vs Δn at $\Delta n = 0$ in Eq. (8), the value of which can be determined from the intercept of the linear fit in Figs. 2d–f.

A difficulty is that this expression also involves J_{0s}/n_i^2, which is in principle unknown. However, because the surface orientation and morphology of the two low-resistivity samples is the same, and because they were processed in parallel, their interface properties should be identical. Here we note that the properties of the Si–Al_2O_3 interface specifically have previously been shown to be independent of substrate doping [48].

Given identical interface properties, $J_{0s}/n_{i,s}^2$ will be independent of doping and injection in the case that $p_s \gg n_s - p_d - n_d + (N_A - N_D)(q\psi_s/kT)$ (for a negative fixed charge Q_f, as in Al_2O_3) [30]. Here p_d and n_d are the hole and electron concentrations at the edge of the quasi-neutral region (identical to the bulk values in the present case), N_A and N_D are the acceptor and donor concentrations, and ψ_s is the surface potential. This condition is fulfilled to within 10 % (that is, p_s is ten times greater than the sum of the other terms) for $|Q_f/q| > 6.0\times10^{11}\,\mathrm{cm^{-2}}$, and to within 1 % for $|Q_f/q| > 2.0\times10^{12}\,\mathrm{cm^{-2}}$ for the investigated dopant concentrations and injection range ($\Delta n < 5\times10^{16}\,\mathrm{cm^{-3}}$). The latter condition is met by the investigated Al_2O_3 films, which are known from capacitance–voltage measurements to have $|Q_f/q| > 2\times10^{12}\,\mathrm{cm^{-2}}$. Note that for Sample #1, which is passivated by a positively charged PO_x/Al_2O_3 stack, the equivalent 1 % condition is $|Q_f/q| > 1.8\times10^{12}\,\mathrm{cm^{-2}}$, well below the measured fixed charge of $|Q_f/q| > 3.7\times10^{12}\,\mathrm{cm^{-2}}$ for such stacks [33,36], so that $J_{0s}/n_{i,s}^2$ can be assumed independent of Δn in that case as well.

In contrast to $J_{0s}/n_{i,s}^2$, J_{0s}/n_i^2 is expected to differ slightly between Samples #2 and #3 due to their different doping, as noted in Section 2. However, at the carrier concentrations considered ($5\times10^{15}\,\mathrm{cm^{-3}} \le \Delta n \le 1.5\times10^{16}\,\mathrm{cm^{-3}}$), this results in a difference of only 1.2 to 2 % based on the bandgap narrowing model of Schenk et al. [49], assuming constant $n_{i,s}$. Fortuitously, this difference is almost precisely compensated in $J_{0s}n_i^{-2}W^{-1}$ by the 1.4 % difference in thickness between Samples #2 and #3.

Given equal $J_{0s}n_i^{-2}W^{-1}$, and assuming negligible bulk SRH recombination, the difference between the intercepts of the linear fit in Figs. 2e and 2f should simply be equal to $C_n n_0 - C_p p_0$. Notice that here the actual value of $(1-f_{reabs,bb})B_{rad}$ is irrelevant, so long as it is the same for both samples. We expect this to be the case to a good approximation for these samples, which are optically identical.

The ratio between C_n and C_p may then be calculated from

$$\frac{C_n}{C_p} = \frac{C_{amb}p_0 + (C_n n_0 - C_p p_0)}{C_{amb}n_0 - (C_n n_0 - C_p p_0)} \tag{16}$$

This results in an initial estimate of $C_n/C_p = 2.47$ based on the values extracted from the as-measured data in Figs. 2e and 2f. Given $C_{amb} = 1.95\times10^{-30}\,\mathrm{cm^6\,s^{-1}}$, we derive values of $C_n = 1.39\times10^{-30}\,\mathrm{cm^6\,s^{-1}}$ and $C_p = 5.6\times10^{-31}\,\mathrm{cm^6\,s^{-1}}$. These initial estimates will be refined in the following section.

4.3. Correcting for bulk SRH and the injection dependence of B_{rad} and $J_{0s}n_i^{-2}$

In using Eq. (8) to extract C_{amb} we have assumed that the terms involving B_{rad} and J_{0s}/n_i^2 are independent of Δn. However, as discussed in Section 2, B_{rad} is in principle dependent on Δn through the two-particle Coulomb-enhancement factor g_{eh}, while J_{0s}/n_i^2 is proportional to $n_{i,s}^2/n_i^2$, which will depend on Δn due to spatially non-uniform bandgap narrowing between the surface space-charge region and the quasi-neutral bulk. Consequently, both terms are expected to decrease somewhat with increasing Δn, which would result in an underestimate of C_{amb} from the slope of $\tau_{eff}^{-1}(p_0+n_0+\Delta n)^{-1}$ vs Δn.

The current accepted model for the injection dependence of B_{rad} in Si is that of Altermatt et al. [8,9],[2] while that for the injection-dependence of n_i is that of Schenk [49,51]. Both are based on first-principles quantum-mechanical calculations. Fig. 3 shows B_{rad} and n_i^{-2} as a function of Δn in intrinsic Si at 300 K according to these models, where we have normalised each to their value at equilibrium. It can be seen that the relative dependence of the two parameters on Δn is remarkably similar. That this is the case is probably not coincidental, since both parameters describe the strength of carrier–carrier screening and were parameterised based on quantum-mechanical calculations

[2] Note that in Eq. 4 of Altermatt et al. [8], b_1 should be replaced with $2b_1$, while b_3 should be replaced with $2b_3$. An attempted correction given in [50] is also in error, citing b_2 instead of b_3. Confirmed by P. P. Altermatt, private communication, May. 2019.

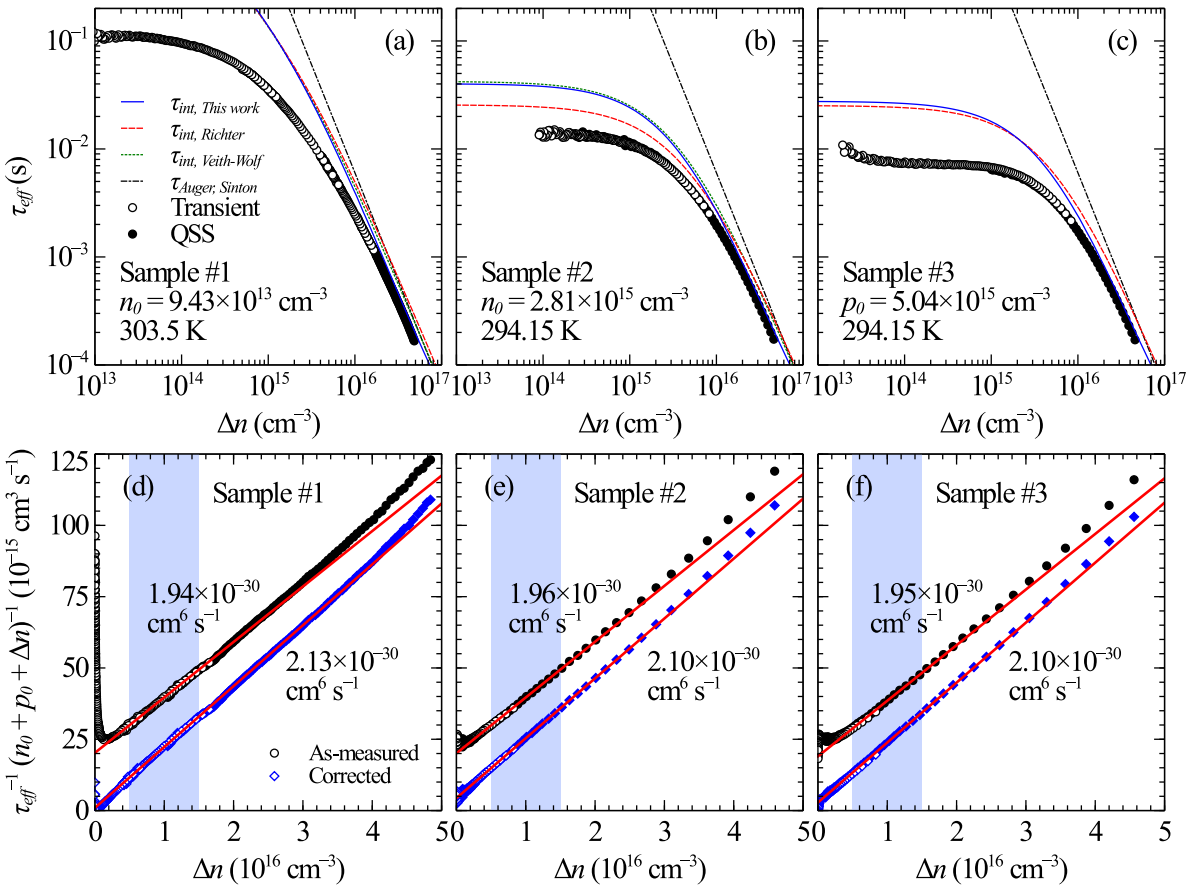

Fig. 2. (a–c) τ_{eff} vs Δn (both on a log scale) for the (a) high-resistivity n-type, (b) low-resistivity n-type, and (c) low-resistivity p-type samples. Dopant concentrations and measurement temperatures are given in the figure. Lines show the corresponding intrinsic lifetime according to the parameterisation of this work, as well as the parameterisations of Richter et al. [1] for n- and p-type, and of Veith-Wolf et al. [19] for n-type, as well as the ambipolar Auger lifetime according to Sinton and Swanson [26]. (d–f) Corresponding $\tau_{eff}^{-1}(p_0 + n_0 + \Delta n)^{-1}$ vs Δn (linear scale) for the same samples, both as-measured, and after subtraction of the (injection-dependent) bulk SRH, surface and radiative components. Lines show linear least-squares fits to the data for 5×10^{15} cm^{-3} $\leq \Delta n \leq 1.5\times10^{16}$ cm^{-3} (this range is indicated by the shaded area). The slope of the fits are given in the figure.

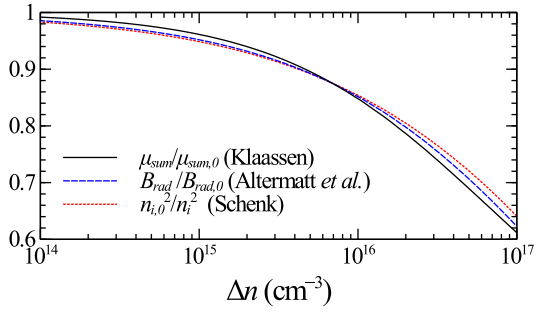

Fig. 3. μ_{sum} according to Klaassen [38], B_{rad} according to Altermatt et al. [8] (with corrections noted in text), and n_i^{-2} according to Schenk [49], as a function of excess carrier concentration Δn in intrinsic silicon at 300 K, normalised to their values at equilibrium.

within a similar theoretical framework. In the case of Altermatt et al., screening was assumed to be described by the Debye potential, while the screening function used by Schenk reduces to the Debye potential at lower concentrations. The coincidence between these models was also noted in the recent publication of Fell et al. [29], who have interpreted it as showing that the $B_{rad}/B_{rad,0}$ model of Altermatt et al. should be treated as a model of bandgap narrowing.

A practical consequence of this near-equality between the injection-dependence of B_{rad} and n_i^{-2} is that in order to account for this dependence, it is not necessary to know the relative magnitudes of the radiative and J_{0s} components in (8), but only their sum. From (8), this can be determined from the $\Delta n = 0$ intercept of the linear fit of $\tau_{eff}^{-1}(p_0+n_0+\Delta n)^{-1}$ vs Δn, as shown in Fig. 2d–e, after subtraction of $C_n n_0$ or $C_p p_0$, which we have already determined to a first approximation.

A complicating factor is that this intercept value also includes bulk SRH recombination, which we have so far neglected. The latter is small in the investigated samples and its presence is not obvious from the plots of τ_{eff} vs Δn in Figs. 2a–c. However, the existence of some amount of bulk SRH recombination is apparent from the slight upward deviation from the linear trend of the $\tau_{eff}^{-1}(p_0 + n_0 + \Delta n)^{-1}$ vs Δn data at low carrier concentrations, as shown in Figs. 2d–f. Besides contributing to the intercept value of $\tau_{eff}^{-1}(p_0 + n_0 + \Delta n)^{-1}$, the general effect of this bulk SRH recombination will be to decrease the slope of $\tau_{eff}^{-1}(p_0 + n_0 + \Delta n)^{-1}$ vs Δn, leading to an underestimate of C_{amb}, in a similar way to the injection dependence of the B_{rad} and J_{0s}/n_i^2 terms. Therefore the problem becomes one of determining and correcting for the separate contributions of bulk SRH and combined radiative/surface recombination. We achieve this by applying an iterative fitting procedure to the data at lower injection levels, as described in Appendix, where the fit was iterated to obtain self-consistency between the input and extracted values of C_n and C_p, as well as equality between J_{0s} for Samples #2 and #3.

Fig. 2d–e shows the final corrected data obtained following subtraction of the bulk SRH and combined radiative/surface recombination components determined using this procedure. Reassessing the slope of this corrected data over the original range of 5×10^{15} cm^{-3} $\leq \Delta n \leq$ 1.5×10^{16} cm^{-3} results in a small increase in the resulting value for

C_{amb} to 2.13×10^{-30} cm^6 s^{-1} for Sample #1, 2.10×10^{-30} cm^6 s^{-1} for Sample #2, and 2.10×10^{-30} cm^6 s^{-1} for Sample #3. Note that these values remain very similar for all samples, despite the difference in doping and temperature. We choose to take the average value of $C_{amb} = 2.11 \times 10^{-30}$ cm^6 s^{-1} as representative of the value at temperatures close to 300 K. Inserting this in (16) together with the difference between the new intercept values for Samples #2 and #3 gives a revised value of $C_n/C_p = 2.81$, leading to $C_n = 1.56 \times 10^{-30}$ cm^6 s^{-1} and $C_p = 5.5 \times 10^{-31}$ cm^6 s^{-1} at ~300 K. We note that this ratio is very close to the ratio $C_n/C_p = 2.83$ resulting from the values reported by Dziewior and Schmid [52] for C_n and C_p at high dopant concentrations.

In Figs. 2a–c we plot the resulting intrinsic lifetime calculated from (7) using these values for C_n and C_p, and assuming $(1 - f_{reabs,bb})B_{rad} = 4.76 \times 10^{15}$ cm^3 s^{-1} [10]. In low injection this results in an intrinsic lifetime slightly higher than that of Richter et al. for the *p*-type sample, and very close to the revised parameterisation of Veith-Wolf et al. for the low-resistivity *n*-type sample. At higher injection levels it results in a lower lifetime than predicted by either of these parameterisations, particularly for the *p*-type sample. This is a consequence of the fractional power dependence of Auger recombination on Δn adopted in these works, which at least in the work of Richter et al. appears to derive largely from the neglect of surface recombination. In fact, a similar overestimation of the high-injection lifetime is apparent in the data presented in Richter et al. (see e.g. Fig. 6 of that work, or our Fig. 8).

4.4. C_n and C_p at high carrier concentrations

We have determined C_p and C_n under conditions where the total free carrier concentration $n + p \leq 3.5 \times 10^{16}$ cm^{-3}. Screening by free carriers is expected to be negligible in this range. Consequently, it is reasonable to assume that these values are also valid at lower carrier concentrations.

At higher carrier concentrations C_p and C_n will be reduced due to screening of the Coulomb enhancement, eventually converging to the values appropriate to the classical case of non-interacting charge carriers. Of the available data [52–56] at these high dopant concentrations (≥~ 10^{19} cm^{-3}), those of Dziewior and Schmid [52] show the least scatter, and have formed the basis for most previous parameterisations in this range. Their reported values of $C_n = 2.8 \times 10^{-31}$ cm^6 s^{-1} and $C_p = 0.99 \times 10^{-31}$ cm^6 s^{-1} are widely accepted. It should be recognised, however, that the work of Dziewior and Schmid was performed over four decades ago, prior to the availability of modern mobility models. They determined the carrier concentration in their samples from the measured resistivity, using the then-standard parameterisation of Irvin [57] for resistivity as a function of total dopant concentration in silicon. The latter was given in the form of piecewise linear approximations to a hand-drawn curve, fit by eye to data from a range of sources for various dopants in Si.

Currently accepted mobility models are based on the more recent measurements of resistivity vs dopant concentration of Thurber et al. in P- and B-doped silicon [42,43], and their extension to higher dopant concentrations and to temperatures other than 300 K by Masetti, Severi, and Solmi [58], and Klaassen [38,39] respectively. For a given resistivity, all of these models predict a carrier concentration in general slightly lower [43] (by ~10 % to 15 % on average, depending on the chosen parameterisation) than the model of Irvin for *n*-type Si at donor concentrations N_D between 10^{18} and 10^{20} cm^{-3}, while for *p*-type Si, they predict a carrier concentration that is similar for N_A in the vicinity of 6×10^{19} cm^{-3}, but substantially lower (by as much as ~50%) in the range of $\sim 3 \times 10^{16}$ cm$^{-3} \leq N_A \leq \sim 3 \times 10^{19}$ cm^{-3} [42].

In principle therefore, the data of Dziewior and Schmid should be reassessed in the light of modern mobility models, and this would be expected to lead in general to lower carrier concentrations and thus to somewhat higher values of C_n and C_p. In Fig. 4 we show the results of such a reassessment, where we have first back-calculated the original measured resistivity ρ of the samples of Dziewior and Schmid based on Irvin's parameterisation, then recalculated n_0 and p_0 using the relationships given by Thurber et al. for $q\rho N$ as a function of N in phosphorus- and boron-doped silicon [42,43]. We choose to use the former relationships in preference to the corresponding parameterisations of mobility provided by Thurber et al., or those of [58] or [38], since the former more closely follow the Hall-effect data of Thurber in the most relevant dopant concentration range (between 10^{19} and 10^{20} cm^{-3}), where this data in turn shows the least scatter among reported values.

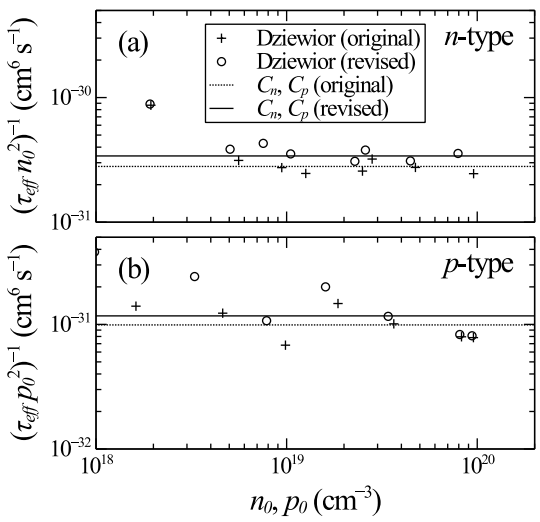

Fig. 4. (a) $\tau_{eff}^{-1} n_0^{-2}$ vs n_0, and (b) $\tau_{eff}^{-1} p_0^{-2}$ vs p_0, as reported by Dziewior and Schmid [52] (crosses) for $p_0, n_0 \geq 10^{18}$ cm^{-3} at 300 K, and as revised using the resistivity vs dopant density relationships for P- and B-doped silicon given by Thurber et al. [42,43] (circles). Lines show (a) C_n, and (b) C_p as reported by Dziewior and Schmid (dashed), and as derived from fits of the revised data at higher concentrations (solid).

We plot the data in the form of $\tau_{eff}^{-1} n_0^{-2}$ vs n_0, and $\tau_{eff}^{-1} p_0^{-2}$ vs p_0, for the *n*- and *p*-type samples respectively, since this results in a quantity with the same units as the Auger coefficients, which allows deviations from the ideal relationship to be more easily perceived than on the usual double-logarithmic scale of lifetime vs majority carrier concentration. Least-squares fits of Dziewior and Schmid's original data (obtained by digitisation of the original figures) resulted in values for C_n and C_p in close agreement (within 2 %) of those reported by them. Similar fits of the revised *n*-type data for n_0 above 10^{19} cm^{-3}, and of the *p*-type data for p_0 above 7×10^{18} cm^{-3}, result in values of $C_n = 3.41 \times 10^{-31}$ cm^6 s^{-1} and $C_p = 1.17 \times 10^{-31}$ cm^6 s^{-1}. Of the two, the greatest uncertainty attaches to C_p, since the *p*-type data show the most scatter. The resulting ratio $C_n/C_p = 2.91$ is only slightly higher than that resulting from the original values.

4.5. The intermediate concentration range

In order to connect the values for C_p and C_n determined at low carrier concentrations with those calculated from the (revised) data of Dziewior and Schmid at high concentrations, we must rely on data for the low-injection lifetime reported in the intermediate doping range by various authors. On the basis of these data we aim to construct expressions for the Coulomb enhancement factors g_{ehh} and g_{eeh} which smoothly connect the former and latter values at each end.

In Fig. 5 we plot a selection of literature data for the low-injection lifetime in *n*- and *p*-type silicon. We plot the data both in the usual form of lifetime vs majority carrier concentration, and as $\tau_{eff}^{-1} n_0^{-2}$ or $\tau_{eff}^{-1} p_0^{-2}$ vs n_0 or p_0, as in Fig. 4.

For *n*-type Si at low concentrations ($n_0 \leq \sim 1.5 \times 10^{16}$ cm^{-3}), significant recent data is available from multiple authors for well-passivated

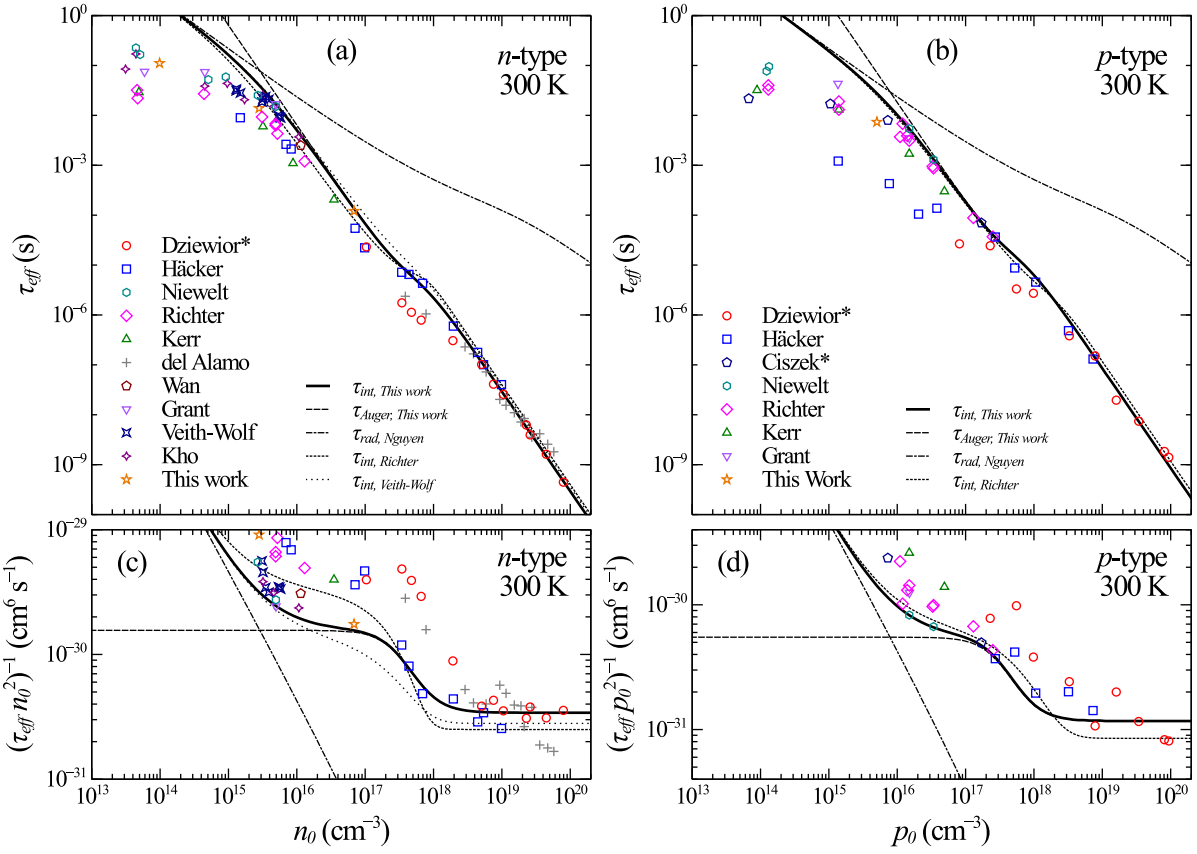

Fig. 5. Summary of low-injection lifetime vs majority carrier concentration reported in the literature for (a) *n*-type, and (b) *p*-type Si at ~300 K. The data of Dziewior and Schmid [52] and Ciszek et al. [59] were reassessed as described in the text. (c) and (d) show the same data replotted as $\tau_{eff}^{-1} n_0^{-2}$ or $\tau_{eff}^{-1} p_0^{-2}$. Lines show the intrinsic and Auger lifetimes according to the parameterisation of this work, the radiative lifetime according to Nguyen et al. [10] with the g_{eh} model of Altermatt et al. [8,9], as well as the intrinsic lifetime according to the parameterisations of Richter et al. [1] for *n*- and *p*-type, and of Veith-Wolf et al. [19] for *n*-type Si.

high-lifetime material [15–21], as noted in the introduction to this work. Meanwhile, at concentrations $n_0 \geq 3 \times 10^{17}\,\mathrm{cm}^{-3}$, the data of Häcker and Hangleiter [3] nicely spans the screening transition and connects with that of Dziewior and Schmid at high concentrations. However, there remains a scarcity of data for well-passivated *n*-type Si in the dopant concentration range between 1.5×10^{16} and $3 \times 10^{17}\,\mathrm{cm}^{-3}$. With the exception of a single data point due to Kerr (for SiO_2-passivated FZ-Si wafers) [60], almost all data in this range is for (relatively thick) unpassivated material, where the surface recombination contribution was assumed negligible due to sample thickness [3,52,53]. That surface recombination was not in fact negligible in these samples is indicated by the fact that all of them exhibit lifetimes significantly lower than is consistent with the upper limits of C_n implied by the most recent measurements of well-passivated *n*-type material at lower concentrations.

We are able to contribute one additional data point in this range, based on our own measurement archive. We have measured a low-injection lifetime of 121 µs for a 251 µm-thick, P-doped *n*-type FZ-Si wafer with $n_0 = 6.88 \times 10^{16}\,\mathrm{cm}^{-3}$ (Sample #4). This sample was passivated by a 20 nm-thick SiO_2 film grown at 1000 °C in dry O_2 and annealed in forming gas at 400 °C for 30 min. The dopant concentration was determined from the dark resistivity of 0.112 Ωcm measured at ~300 K by the same carefully calibrated photoconductance coil used to perform the lifetime measurements of Sample #1, using the mobility model of Klaassen. The near-surface dopant concentration was separately determined from combined high-frequency/quasi-static capacitance–voltage (C–V) measurements of metal–insulator–semiconductor dot-contact structures prepared on the same wafer after SiO_2 growth, using the method of [61]. This resulted in an average value $N_A = 8.20 \times 10^{16}\,\mathrm{cm}^{-3}$, measured at a depth of ~80–95 nm from

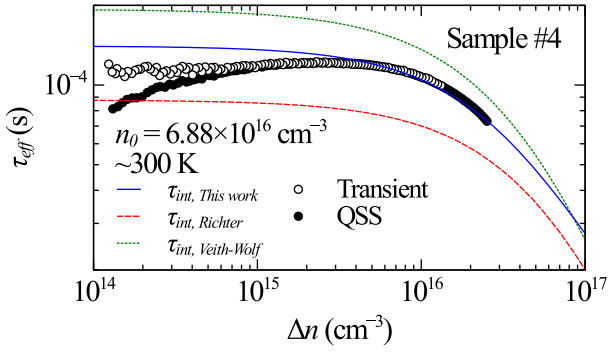

Fig. 6. τ_{eff} vs Δn measured for an SiO_2-passivated *n*-type FZ-Si sample with $n_0 = 6.88 \times 10^{16}\,\mathrm{cm}^{-3}$. Lines show the corresponding intrinsic lifetime according to the parameterisations of Richter et al. [1], Veith-Wolf et al. [19], and this work. In the latter case we have included the effects of photon recycling.

the surface (as determined from the depletion region width at the extraction point). This slightly higher value is qualitatively consistent with the expected P-dopant pile-up at this depth due to the oxidation process. As shown in Fig. 6, the resulting lifetime is significantly higher than the intrinsic lifetime given by Richter et al. at this concentration, but we expect it still to be an underestimate of the true bulk lifetime, since surface recombination in this sample was certainly not negligible.

For *p*-type silicon, the best lifetimes reported in the low-to-intermediate range ($p_0 \leq \sim 1.5 \times 10^{17}\,\mathrm{cm}^{-3}$) are those recently reported by Niewelt et al. [18], along with those of Richter et al.. Together, these provide better coverage of this range than available for *n*-type silicon.

High-lifetime data in this range is also available from the older work of Ciszek et al. [59], who measured lifetime in Ga-doped ingots. We have reassessed the values of p_0 for the latter data from the original reported resistivities using Eq. 2 of [42], which is in excellent agreement with more recently reported data for carrier concentration vs resistivity in Ga-doped silicon [62]. Notably, this correction brings the errant data point of Ciszek et al. at $\sim 1.7 \times 10^{17}$ cm^{-3} (previously 3×10^{17} cm^{-3}), which had been a high-lifetime outlier in previous reviews, into line with the data of Richter et al. and Häcker and Hangleiter in this region. The latter data again covers the transition region and links up with the data of Dziewior and Schmid at high concentrations.

4.6. Coulomb enhancement factors

The larger values of C_n and C_p observed at low carrier concentrations in silicon have been explained as being due to spatial correlation of the electron and hole populations due to Coulombic attraction [3,32]. This Coulomb enhancement effect is effectively screened at higher carrier concentrations, eventually converging to the ideal free-particle limit. As pointed out by Altermatt et al. [12,13], the screened Coulomb potential is described to a first approximation by the Debye potential, which is a function of the sum of the free carrier concentrations $p + n$. Consequently, the Coulomb-enhancement factors g_{eeh} and g_{ehh} should also be a function of $p + n$, including both equilibrium and non-equilibrium carriers.

The question then arises as to the appropriate form of the expression describing g_{eeh} and g_{ehh}. Only very limited guidance from theory is available on this point. The theoretical results of Hangleiter and Häcker [32] for low-injection conditions at 300 K are in poor agreement both quantitatively and qualitatively with the experimental data. Meanwhile, the available low-injection lifetime data in the transition region is sufficiently sparse to permit multiple similarly good descriptions based on different empirical functions. Richter et al. used the following three-parameter empirical expression, which was originally proposed by [4] (here we have substituted $p + n$ for n_0 or p_0 in the original formulation).

$$g_i = 1 + (g_{max,i} - 1)\left(1 - \tanh\left[\left\{\frac{p+n}{N_{0,i}}\right\}^{\theta_i}\right]\right) \tag{17}$$

where $g_{max,i}$ is the value of the Coulomb enhancement factor at low carrier concentrations, $N_{0,i}$ is a reference concentration, and θ_i is an arbitrary exponent which determines the sharpness of the transition. Here the subscript i stands in for *eeh* or *ehh*.

This expression can describe the transition well on the high-concentration side, where it is most tightly constrained by the available data. However, a difficulty with this expression is that it predicts a relatively slow saturation of g_{eeh} and g_{ehh} at low concentrations, as a consequence of the behaviour of tanh. Consequently, if this expression is also employed to describe the dependence of the Coulomb enhancement on the non-equilibrium carrier concentration, it will predict a rather significant dependence of C_{amb} on Δn within the range commonly probed in photoconductance lifetime measurements. This contradicts the data of Fig. 2, which does not support a significant dependence of C_{amb} on Δn in this range.

An alternative, similarly empirical, three-parameter expression to describe the Coulomb enhancement factors was suggested by Jonsson et al. [63]:

$$g_i = 1 + (g_{max,i} - 1)\left(1 + \left[\frac{p+n}{N_{0,i}}\right]^{\theta_i}\right)^{-1} \tag{18}$$

This expression results in a transition that is more symmetrical on the high- and low-concentration ends with respect to $\log(p + n)$ than (17). This makes it compatible with a more rapid saturation of the enhancement factor with decreasing carrier concentration (or, looked at another way, a higher concentration for the onset of significant screening), while maintaining a similar dependence at high concentrations. For this reason, we consider it preferable to (17).

We note that both (17) and (18) are limiting cases of the generalised (five-parameter) logistic function, where in the case of (17) the variable is the carrier concentration, and in (18) its logarithm. Other more-or-less simplified variants of this function could in principle be chosen. Indeed, a five-parameter asymmetric logistic function was used by Altermatt et al. [8] to parameterise the two-particle Coulomb enhancement factor for radiative recombination in silicon. However, the additional degrees of freedom obtained by increasing the number of fitting parameters are currently difficult to justify given the scatter of the available experimental data.

Table 2
Parameter values for (18), (19) in the Auger model of this work.

Parameter	Value	Units
C_{p0}	1.17×10^{-31}	cm^6 s^{-1}
C_{n0}	3.41×10^{-31}	cm^6 s^{-1}
$g_{max,ehh}$	4.74	–
$g_{max,eeh}$	4.57	–
$N_{0,ehh}$	3.2×10^{17}	cm^{-3}
$N_{0,eeh}$	3.2×10^{17}	cm^{-3}
θ_{ehh}	2	–
θ_{eeh}	2	–

4.7. Generalised expression for Auger recombination in c-Si

Based on our own results and the available literature data, we propose the following generalised model for the Auger lifetime in crystalline silicon as a function of the electron and hole concentrations

$$\tau_{Auger} = \Delta n[g_{ehh}C_{p0}(p^2 n - p_0^2 n_0) + g_{eeh}C_{n0}(pn^2 - p_0 n_0^2)]^{-1} \tag{19}$$

with $g_{eeh}(p + n)$ and $g_{ehh}(p + n)$ given by (18), and where the values of all parameters are given in Table 2.

The resulting modelled Auger lifetime τ_{Auger}, as well as the total intrinsic lifetime τ_{int} assuming $(1 - f_{reabs,bb})B_{rad} = 4.76 \times 10^{15}$ cm^3 s^{-1} [10], is shown in Fig. 5a–d as a function of n_0 and p_0 under low-injection conditions at 300 K. The model may be most conveniently compared with the available experimental data when plotted as $\tau_{eff}^{-1} n_0^{-2}$ or $\tau_{eff}^{-1} p_0^{-2}$ vs n_0 or p_0, as in Figs. 5c and 5d.

At the highest carrier concentrations ($n_0, p_0 > \sim 10^{19}$ cm^{-3}) our fit is based on the data of Dziewior and Schmid, as revised in Fig. 4. In this range we consider that Auger recombination is likely dominant, and that remaining scatter in the literature data is therefore due to (random) experimental uncertainties. Consequently, it is appropriate for the fit to follow the average value of the literature data in this range. Here the parameterisation of this work predicts a significantly lower lifetime (or higher values of C_{n0} and C_{p0}) than the model of Richter et al. for both *n*- and *p*-type silicon. This is partly because Richter et al. based their fit on the original data of Dziewior and Schmid, whereas we base our fit on the revised data, which results in lower values of $(\tau_{eff} n_0^2)^{-1}$ and $(\tau_{eff} p_0^2)^{-1}$, and partly because Richter et al. appear to have based their fit on the highest lifetime values in this range rather than the average (their values of $C_{n0} = 2.5 \times 10^{-31}$ cm^6 s^{-1} and $C_{p0} = 8.5 \times 10^{-32}$ cm^6 s^{-1} are lower than those reported by Dziewior and Schmid).

At low carrier concentrations, our fit is based on the low-concentration values of C_n and C_p determined experimentally in this work. The extrapolation of these values to even lower values of n_0 and p_0 is justified by the fact that in this range the enhancement function is expected [9] simply to reduce to that given by the unscreened Coulomb potential [64]. The ratios of these values to C_{n0} and C_{p0} respectively define the values of $g_{max,eeh} = 4.57$ and $g_{max,ehh} = 4.74$. The latter values

are noticeably quite close to equal. This is in contrast to the parameterisation of Richter et al., where $g_{max,eeh}$ was more than 60 % larger than g_{ehh}. This is primarily a consequence of the significantly lower value of C_n determined in this work, which is consistent with more recent literature data. In principle, there is no physical reason to expect that $g_{max,eeh}$ and $g_{max,ehh}$ should differ significantly. According to Hangleiter and Häcker [32], their ratio should depend approximately on the ratio of the electron–electron and hole–hole two-particle correlation factors (g_{ee}/g_{hh}), although this conclusion is based on the assumption that g_{eeh} and g_{ehh} can be derived from the linear superposition of the two-particle correlation terms, which ignores compensation effects known to occur in many-particle systems [65]. Within the constraints of the fit imposed by the available data, it would be feasible to set them to be equal. However, since significant uncertainty still attaches to the values at both low and high concentrations (particularly for the *ehh* process), it appears preferable to continue to treat them as independent fitting parameters for the time being.

At intermediate concentrations ($\sim 10^{17}\ \mathrm{cm^{-3}} \leq n_0, p_0 \leq \sim 10^{19}\ \mathrm{cm^{-3}}$), in the transition region, the influence of surface and bulk SRH recombination cannot be ruled out. In this range the majority of high-lifetime data available is that of Häcker and Hangleiter, which was certainly affected by extrinsic recombination at concentrations less than $\sim 10^{17}$ $\mathrm{cm^{-3}}$ as discussed above. We therefore consider the literature data as a lower bound on τ_{int}, or upper bound on $\tau_{int}^{-1} n_0^{-2}$ or $\tau_{int}^{-1} p_0^{-2}$. At the same time, the data is still clearly subject to experimental uncertainty, especially regarding concentration values. Therefore we do not attempt to fit it overly closely. Instead, noting that there is no physical reason to expect the concentration dependence of the screening functions for the *eeh* and *ehh* processes to differ considerably, we set $N_{0,eeh} = N_{0,ehh}$ and $\theta_{eeh} = \theta_{ehh}$, and vary these values in order to provide a reasonable fit to both data sets simultaneously, placing more weight on the more recent literature data of Richter et al. than on the data of Häcker and Hangleiter.

Fig. 5c shows that our new parameterisation predicts significantly higher low-injection lifetimes than that of Richter et al. in *n*-type Si at lower carrier concentrations, particularly for $10^{15}\ \mathrm{cm^{-3}} \leq n_0 \leq 3 \times 10^{17}\ \mathrm{cm^{-3}}$. In this it is consistent with the mass of more recent literature data at these concentrations. It agrees closely with the parameterisation of Veith-Wolf et al. for $n_0 \leq 10^{16}\ \mathrm{cm^{-3}}$, but deviates significantly at higher values of n_0, where it more closely follows the experimental data through the transition region. This is a (probably unintended) consequence of the retention by Veith-Wolf et al. of the same values for $N_{0,eeh}$ and θ_{eeh} as Richter et al. in (17) while changing $g_{max,eeh}$.

For *p*-type Si (Fig. 5d), our parameterisation predicts slightly higher lifetimes than that of Richter et al. for $10^{16}\ \mathrm{cm^{-3}} \leq n_0 \leq 2 \times 10^{18}\ \mathrm{cm^{-3}}$. From $10^{16}\ \mathrm{cm^{-3}}$ to $2.5 \times 10^{17}\ \mathrm{cm^{-3}}$ it is fairly tightly bounded by the data of Richter et al., Niewelt et al., and revised data of Ciszek et al.

It should be borne in mind that τ_{int} in Fig. 5 is calculated assuming $f_{reabs,bb} = 0$, i.e. that photon recycling is negligible, while the experimental data certainly includes some degree of photon recycling [29], which will reduce the effective contribution of the radiative component. Therefore measured lifetimes above this value of τ_{int} but below τ_{Auger} are possible.

5. Discussion

5.1. Influence of the mobility model

The largest source of uncertainty in the analysis lies in the assumed mobility model used to relate the measured sample conductance to carrier concentration. In particular, while the dependence of the equilibrium majority-carrier mobility on carrier concentration and temperature in silicon has been measured with high precision, the injection dependence of the non-equilibrium carrier mobilities is known with a lesser degree of confidence. Only a small number of experimental

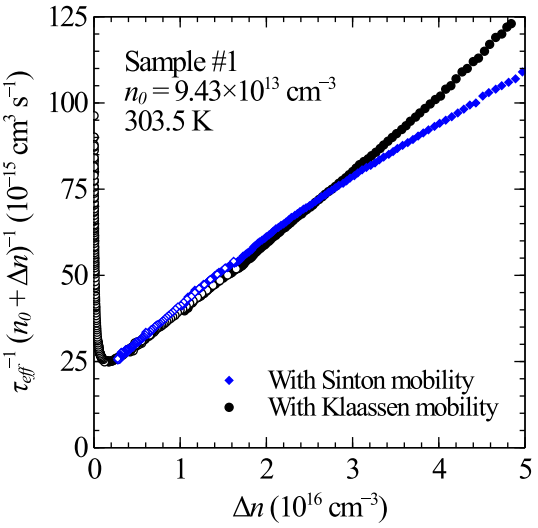

Fig. 7. $\tau_{eff}^{-1}(n_0+\Delta n)^{-1}$ vs Δn for Sample #1 ($n_0 = 9.43 \times 10^{14}\ \mathrm{cm^{-3}}$), as calculated using either the mobility model of Klaassen (at the measurement temperature of 303.5 K) or the empirical parameterisation of Sinton.

determinations of this dependence have been made [40,41,46,66–70], generally for the high-injection case ($\Delta n \gg p_0, n_0$). The most extensive dataset is that of Dannhäuser and Krausse, which in the lower concentration range was based on measurements of the voltage drop on switching from forward to reverse bias in electrically injected *pn* junction diodes at (undefined) room temperature. The resulting data show significant scatter, as can be seen in Fig. 1. At higher concentrations they may have been affected by sample heating as suggested by Klaassen [38].

Existing models [13,38,39,66,68,71] for the injection-dependence of the mobility sum $\mu_{sum} = \mu_p + \mu_n$ in silicon show significant divergence at higher values of Δn. Lower (higher) values of the mobility lead to higher (lower) apparent values of Δn for a given sample conductance, resulting in increased (decreased) estimates of C_{amb} from the slope of $\tau_{eff}^{-1}(p_0 + n_0 + \Delta n)^{-1}$ vs Δn.

Fig. 7 shows the effect of the choice of mobility model on $\tau_{eff}^{-1}(n_0 + \Delta n)^{-1}$ vs Δn of Sample #1. The data are shown as calculated either (i) using the mobility model of Klaassen at the measurement temperature (303.5 K), as in Fig. 2d, or (ii) using Sinton's empirical parameterisation of μ_{sum}, which is based on the room-temperature data of Dannhäuser and Krausse. Note that in the latter case the optical constant C_{opt} was also adjusted to maintain self-consistency between the data measured under transient and QSS conditions, which tends to partially compensate the effect of the change in mobility.

In general, there is fairly good agreement between the data calculated with both mobility models for $\Delta n \leq \sim 3 \times 10^{16}$ $\mathrm{cm^{-3}}$. This reflects the close agreement between the mobility models in this range at this temperature (see Fig. 1). However, the data derived based on the Sinton mobility model show a ~10% larger slope ($2.15 \times 10^{-30}\ \mathrm{cm^6\ s^{-1}}$ vs $1.94 \times 10^{-30}\ \mathrm{cm^6\ s^{-1}}$) for $5 \times 10^{15}\ \mathrm{cm^{-3}} \leq \Delta n \leq 1.5 \times 10^{16}\ \mathrm{cm^{-3}}$, together with a significant deviation from linear behaviour with reduced slope for $\Delta n \geq \sim 2 \times 10^{16}\ \mathrm{cm^{-3}}$. The latter, if real, could be interpreted as evidence for the onset of screening of the Coulomb enhancement. Accurate, temperature-controlled measurements of the non-equilibrium mobility in modern high-purity silicon material would be helpful to adjudicate between the different mobility models in this range.

Note that the initial larger slope of the data derived using the Sinton mobility parameterisation, which would result in a larger estimate of C_{amb}, is partly a consequence of the fact that this parameterisation does not take into account the temperature dependence of the mobility, which is significant even for small deviations around 300 K. For Samples #2 and #3, which were measured at a lower temperature than

Sample #1, the application of the Sinton mobility parameterisation instead results in a smaller initial slope of $\tau_{eff}^{-1}(n_0+p_0+\Delta n)^{-1}$ vs Δn than the model of Klaassen (e.g. 1.88×10^{-30} cm^6 s^{-1} vs 1.96×10^{-30} cm^6 s^{-1} in the case of Sample #2). The use of a temperature-independent mobility model therefore produces a significant apparent temperature-dependence in C_{amb}, the major part of which however appears in fact to be an artefact of the temperature dependence of the mobility. The use of mobility models which account for temperature, together with accurate measurements of the sample temperature during the measurement, are thus important for accurate extraction of the Auger coefficients from photoconductance measurements.

5.2. Assumption of carrier uniformity

In our analysis, we have implicitly assumed that Δn is spatially uniform both over the measurement area and throughout the depth of the sample. If Δn were non-uniform, the apparent value Δn_{app} calculated from the total measured conductance would be approximately equal to the average value (for small departures from uniformity). Since the total recombination increases non-linearly with Δn, this would lead to an overestimation of the recombination corresponding to a given value of Δn_{app}.

Since the generation rate is depth-dependent, Δn may be non-uniform throughout the depth of the sample for short times following transient excitation, or under steady-state conditions when the diffusion length is comparable to or smaller than the sample thickness. These conditions are most likely to occur at high Δn, where the lifetime and diffusion length are shorter. To evaluate the impact of non-uniformity in the carrier profile, we model the carrier profile under quasi-steady-state conditions using the QSS-Model software [72,73], which we modified to use our Auger model for self-consistency.

The modelling shows that at an apparent injection level $\Delta n_{app} = 5\times10^{16}$ cm^{-3}, Δn at the front of Sample #1 is 15 % greater than at the rear. However, this nonuniformity translates into an overestimation of the corresponding $\tau_{eff}^{-1}(\Delta n_{app})$ of only 1.4 %. Furthermore, this error reduces with decreasing Δn_{app}. For instance, at $\Delta n_{app} = 2\times10^{16}$ cm^{-3}, the overestimation of $\tau_{eff}^{-}1(\Delta n_{app})$ is only 0.13 %. Consequently the influence of carrier profile non-uniformities can be neglected in the present study.

Lateral uniformity was verified for Sample #1 using photoluminescence (PL) imaging at a range of excitation intensities. Steady-state PL intensity was calibrated to Δn in the manner described in our previous work [35], and assessed over the 3 cm diameter region surrounding the position of the inductive coil in the photoconductance lifetime measurements. This region accounts for 98 % of the sensitivity of the photoconductance coil [28]. Mean Δn as well as mean $\tau_{eff}^{-1} \propto \Delta n^{-1}$ were assessed, and the latter was compared to τ_{eff}^{-1} corresponding to the mean Δn.

Lateral non-uniformity was greatest at the lowest excitation intensities, corresponding to the lowest Δn, where longer carrier diffusion lengths allow low-lifetime regions to influence recombination over greater distances. At an average Δn of ~10^{15} cm^{-3}, the standard deviation of Δn over the measurement area was ~9% of the mean value. However, this resulted in a mean value of τ_{eff}^{-1} that was still less than 1 % greater than the value corresponding to the mean Δn. Lateral non-uniformities decreased significantly at higher excitation levels. Therefore the influence of lateral non-uniformity is also negligible for Sample #1.

5.3. Other lifetime measurement techniques

In this work we have proposed an approach to determine the Auger coefficients from measurements of $\tau_{eff}(\Delta n)$, on the basis of Eq. (8). We chose to determine $\tau_{eff}(\Delta n)$ via inductively-coupled photoconductance decay measurements, however in principle the same analysis could be applied to $\tau_{eff}(\Delta n)$ measured using other techniques, for instance photoluminescence [74,75] or open-circuit voltage decay [26] (OCVD). In this case the relevant material property relating the measured quantity to Δn would change from the mobility to the radiative coefficient B_{rad} or the intrinsic carrier concentration n_i respectively.

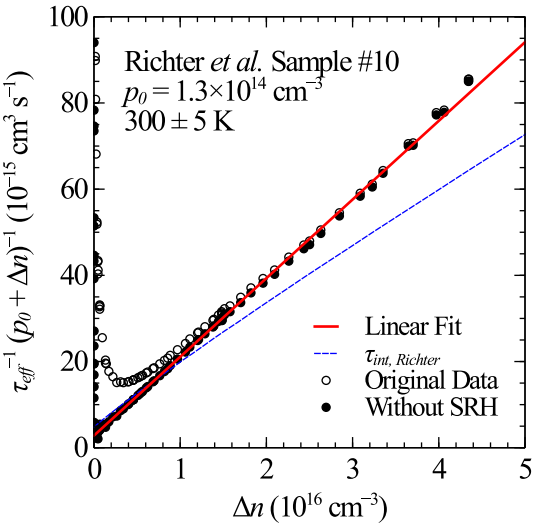

Fig. 8. $\tau_{eff}^{-1}(p_0+\Delta n)^{-1}$ vs Δn reported by Richter et al. [1] for their Sample #10 ($p_0 = 1.3\times10^{14}$ cm^{-3}), which was measured using the steady-state PL technique. The same data is also shown after subtracting the fitted bulk SRH component. Lines show a linear least-squares fit to the data for 5×10^{15} cm$^{-3} \le \Delta n \le 1.5\times10^{16}$ cm^{-3} and the corresponding intrinsic lifetime according to the parameterisation of Richter et al..

As an example of the application of our approach to exemplary lifetime data measured using the PL technique, in Fig. 8 we plot $\tau_{eff}^{-1}(p_0+\Delta n)^{-1}$ vs Δn for Sample #10 of Richter et al. [1] (the highest-lifetime sample in that study), which was measured by the steady-state PL technique [75], calibrated using the self-consistent quasi-steady-state photoluminescence (QSSPL) method of Trupke et al. [74]. We plot the data both as-measured and after the subtraction of the bulk SRH component (determined by fitting the data in low injection). Notably, the data follow an essentially linear dependence within the measured range (up to ~4×10^{16} cm^{-3}), suggesting that C_{amb} is independent of Δn in this range. This is consistent with our photoconductance data analysed using the mobility model of Klaassen (Fig. 2). A linear fit in the range 5×10^{15} cm$^{-3} \le \Delta n \le 1.5\times10^{16}$ cm^{-3} gives a slope of 1.83×10^{-30} cm^6 s^{-1}, slightly lower than our value. Fig. 8 also shows the intrinsic lifetime according to the parameterisation of Richter et al., which is sub-linear as a consequence of the fractional dependence of the ambipolar Auger component on Δn adopted in that work, and clearly deviates significantly from the data at higher carrier concentrations.

As an example of exemplary OCVD lifetime data, in Fig. 9 we plot $\tau_{eff}^{-1}\Delta n^{-1}$ vs Δn calculated from the OCVD data measured by Sinton and Swanson [26] in specially designed point-contact cell structures, which they used to determine their value for the ambipolar Auger coefficient. Sinton and Swanson analysed their data using a value for n_i significantly higher (1.45×10^{10} cm^{-3} at 300 K) than currently accepted values [51,76], and did not consider bandgap narrowing. We plot their data both as assessed using their original value of n_i, and as reassessed with n_i of Couderc, Amara, and Lemiti [76], and the bandgap narrowing model of Schenk [49]. $\tau_{eff}^{-1}\Delta n^{-1}$ is significantly higher for the revised data due to the lower value of n_i. We also plot the revised data after subtraction of the bulk SRH and J_0 components determined by fitting the injection dependence. A linear fit to the corrected data over the full range gives a slope of 2.65×10^{-30} cm^6 s^{-1}, significantly higher than our value for C_{amb} or the original value of 1.66×10^{-30} cm^6 s^{-1} of Sinton and Swanson. We note that a similar treatment of the original data gave 1.65×10^{-30} cm^6 s^{-1}, essentially identical to the original value.

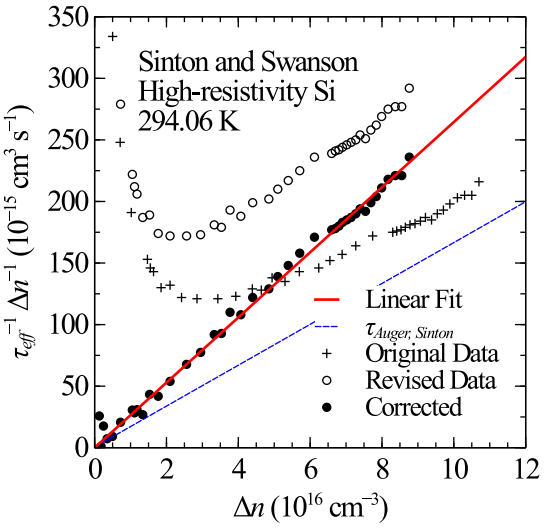

Fig. 9. $\tau_{eff}^{-1}\Delta n^{-1}$ vs Δn measured by Sinton and Swanson [26] in high-resistivity silicon using the open-circuit voltage decay technique, analysed both with the original value for n_i, and as revised using the n_i model of Couderc, Amara, and Lemiti [76] and bandgap narrowing model of Schenk [49]. The revised data is also shown after subtracting the fitted bulk SRH and J_0 components. Lines show a linear least-squares fit to the corrected data over the full range, as well as the ambipolar Auger lifetime according to Sinton and Swanson.

The value of C_{amb} extracted using (8) depends, in high injection, on the slope of $\tau_{eff}^{-1}\Delta n^{-1}$ vs Δn. For steady-state measurements, τ_{eff} is itself proportional to Δn, and so $C_{amb} \propto \Delta n^{-3}$, while for transient measurements, $C_{amb} \propto \Delta n^{-2}$. For photoconductance measurements, $\Delta n^{-2} \propto \mu_{sum}^2$. Similarly, for photoluminescence measurements, $\Delta n^{-2} \propto B_{rad}$, while for open-circuit voltage measurements $\Delta n^{-2} \propto n_i^{-2}$. The accuracy of the extracted value of C_{amb} thus depends critically on the accuracy with which the values of these properties are known. For instance, a 12 % increase in the value of n_i would be sufficient to bring C_{amb} from the data of Sinton and Swanson into agreement with our value.

The accuracy of existing models for both B_{rad} and n_i in silicon are subject to similar experimental uncertainties as the mobility. This is particularly the case when it comes to the dependence of both quantities on Δn. Currently available models [8,49] for the dependence of B_{rad} and n_i on Δn are based on quantum-mechanical calculations involving different levels of approximation, and have not been extensively verified experimentally. As shown in Fig. 3, they predict a significant dependence of these properties on Δn in the range normally probed by lifetime measurements. This has a significant effect on the extracted values of τ_{eff} and Δn, especially at higher injection levels. Therefore, in order to further narrow down estimates of C_{amb}, it will be essential to experimentally verify, and if necessary revise, the existing models for the injection dependence of B_{rad} and n_i as well as mobility.

Given the temperature dependence of these parameters, accurate measurement of sample temperatures during lifetime measurements will also be critical to reduce remaining uncertainties. Even assuming the accuracy of current models for n_i, the aforementioned 12 % increase in n_i required to bring C_{amb} from the data of Sinton and Swanson into agreement with our own would be obtained given only a 1.4 K error in the sample temperature, thanks to the strong temperature-dependence of n_i. There is therefore a significant advantage in using lifetime measurement techniques in which the relevant material parameter is less sensitive to sample temperature, such as photoconductance and especially PL measurements (while noting that the latter measurements are somewhat more difficult to calibrate).

5.4. Recommendations

In this work, we have developed a full Auger parameterisation largely as a vehicle to explore various considerations relevant to future revisions of the Auger model in silicon (which are to be expected). Nevertheless, we believe this parameterisation is a clear improvement over the currently accepted parameterisation of Richter et al., in that it (i) is consistent with the more recent literature data at low doping levels in *p*- and especially *n*-type silicon, (ii) better describes the revised data of Dziewior and Schmid at high doping levels, (iii) treats recombination involving equilibrium and non-equilibrium carriers on the same basis, and (iv) features close symmetry between the enhancement factors for *eeh* and *ehh* processes, consistent with physical expectations.

The revised parameterisation has consequences for the theoretical efficiency limit of crystalline silicon solar cells. Specifically, compared to the parameterisation of Richter et al., the revised parameterisation predicts somewhat higher Auger recombination in undoped silicon in the injection level range corresponding to the maximum power point at one Sun, and this will result in a slight reduction in the maximum efficiency limit. Conversely, for moderately doped Si (i.e. 1 Ωcm resistivity) the revised parameterisation predicts slightly lower Auger recombination in the relevant injection range for *p*-type Si, and significantly lower for *n*-type Si. This will tend to increase the efficiency limits for doped material, especially *n*-type.

At high doping levels the revised parameterisation predicts significantly higher Auger recombination in both *n* and *p*-type Si than previous parameterisations (36 % to 38 % higher compared to that of Richter et al.), due to our reassessment of the data of Dziewior and Schmid. Note that consequently it should not be used in combination with empirical models that were derived based on measurements sensitive to Auger recombination in this range, where another Auger parameterisation was used in the analysis, for example bandgap narrowing models or parameterisations of the surface recombination velocity based on measurements of J_0 at *passivated* diffused surfaces, e.g. [77,78]. On the other hand, it can still be used with empirical bandgap narrowing models based on measurements of J_0 at *metallised* diffused surfaces, such as those of Yan and Cuevas [79,80], since such measurements are relatively insensitive to Auger recombination.

The revised parameterisation will affect values of J_0 extracted from the slope of $\tau_{eff}^{-1} - \tau_{int}^{-1}$ vs Δn via the method of Kane and Swanson [27]. Compared to the Auger parameterisations of both Sinton and Swanson, and Richter et al., the revised parameterisation will generally result in smaller extracted values of J_0, due to its larger injection-dependent Auger component. The magnitude of the difference will depend on the thickness and doping of the sample, and the injection level chosen for extraction, but will typically be on the order of 1–2 fA cm^{-1}, and will decrease with decreasing injection level. Use of the revised parameterisation is also generally expected to result in a more linear plot of $\tau_{eff}^{-1} - \tau_{int}^{-1}$ vs Δn than when using the parameterisations of Sinton and Swanson or Richter et al., especially for well-passivated samples. Note that, given the uncertainty in the existing mobility models, the extraction of J_0 from photoconductance data is best performed at injection levels below 1.5×10^{16} cm^{-3}.

The new parameterisation rests on the low-concentration value of C_{amb}, which is the parameter determined most directly. The accuracy of this value depends mainly on the accuracy of the mobility model of Klaassen in the relevant injection range. As noted above, in this range Klaassen's mobility model is in good agreement with both Sinton's parameterisation and the experimental data of Dannhäuser and Krausse.

The largest uncertainties in the parameterisation are in the value for C_p at low concentrations (due to significant uncertainty in C_n/C_p, and the smaller value of C_p compared to C_n), (ii) C_{p0} at high concentrations (due to significant scatter in the data of Dziewior and Schmid), and (iii) the exact dependence of the Coulomb enhancement in the transition region (due to the limited available data in the relevant range).

We are aware of a separate, shortly forthcoming revision of the Auger parameterisation by Niewelt et al. [25] (indeed, one of the current authors is also a co-author on this latter work). Though this work is essentially independent, it takes on board several aspects of our approach, including our revised values for C_{p0} and C_{n0}, and the form of the Coulomb-enhancement functions. The resulting parameterisation is quite similar to our own. We expect that the low-concentration values of C_n and particularly C_p in the parameterisation of [25] should be more reliable than ours, since they are based on a significantly larger dataset with state-of-the-art sample preparation, and systematic exclusion of surface recombination via sample thickness variation. On the other hand, our value for $C_{amb} = C_n + C_p$ shows significantly less scatter between different samples—likely because we account for the temperature dependence of the mobility and the injection dependence of the equilibrium carrier conductance—and may be more accurate. However, the difference is within the uncertainty due to the underlying mobility models. We therefore recommend the parameterisation of Niewelt et al. for general use, while encouraging future studies aimed at further refining the Auger parameterisation to take such factors into account.

6. Conclusion

We have proposed an approach to measure the ambipolar Auger coefficient $C_{amb} = C_n + C_p$ in crystalline silicon by exploiting the distinct injection dependence of the various recombination components, in particular the now-well-understood injection-dependence of J_{0s} at surfaces passivated by dielectric materials with a large interface fixed charge. We have applied this approach to carefully calibrated photoconductance measurements of several well-passivated samples, taking advantage of recent improvements we have demonstrated in the accuracy of such measurements, and accounting for factors usually neglected, such as the temperature dependence of the mobility and the injection dependence of the equilibrium carrier conductance. The obtained value of $C_{amb} = (2.11 \pm 0.02) \times 10^{-30}\,\mathrm{cm^6\,s^{-1}}$ was found to be independent of dopant concentration for moderately doped p- and n-type samples near 300 K. By exploiting the near-independence of J_{0s} on doping across identically processed samples, we furthermore obtained an estimate of the ratio $C_n/C_p = 2.81$ at low carrier concentrations, which is close to the value 2.91 determined from the reassessed data of Dziewior and Schmid at high doping levels. We have shown that a comprehensive Auger parameterisation consistent with these results, with equilibrium and non-equilibrium carriers treated on the same basis, and close symmetry between the Coulomb enhancement functions for electrons and holes, is both feasible and consistent with the available literature data. In doing so, we have sought to highlight a number of experimental considerations which will be relevant for future efforts to further refine the Auger parameterisation in silicon, as well as areas where data is currently lacking, or where confirmation of or adjudication between existing models is required.

CRediT authorship contribution statement

Lachlan E. Black: Conceptualisation, Methodology, Software, Formal analysis, Investigation, Writing – original draft, Visualisation. **Daniel H. Macdonald:** Writing – review & editing, Funding acquisition.

Declaration of competing interest

The authors declare that they have no known competing financial interests or personal relationships that could have appeared to influence the work reported in this paper.

Acknowledgement

This work was supported by the Australian Renewable Energy Agency (ARENA) through project RND017. The authors gratefully acknowledge Marco Ernst, Roel J. Theeuwes, Simeon Baker-Finch and Teng Kho for assistance with sample preparation, and Vincent Vandalon for assistance with four-point-probe measurements. Armin Richter and Ronald A. Sinton generously shared their original measurement data. We are also indebted to Ronald A. Sinton and Pietro P. Altermatt for valuable discussions, and to Tim Niewelt for providing feedback on the draft text.

Appendix. Procedure used to correct for bulk SRH, and injection dependence of radiative and J_{0s} components

The following procedure was used to determine and correct for the SRH, radiative, and J_{0s} components:

1. C_{amb} and C_n/C_p were fixed to their initial estimated values.
2. τ_{eff}^{-1} was fit for $\Delta n \leq 5 \times 10^{15}\,\mathrm{cm^{-3}}$ using (7), where τ_{SRH} was calculated using the SRH formalism for a single-level mid-gap defect, and the radiative and J_{0s} components were consolidated into a single term $(\tau_{rad}^{-1} + \tau_s^{-1})\Delta n = B_{total}(n_{i,0}^2/n_i^2)pn$. The fitting parameters were thus B_{total} and the SRH lifetimes for majority and minority carriers. The fit range was chosen as approximately that in which the sum of the radiative and surface recombination components were larger than the Auger component for these samples. This helps to limit the sensitivity of the fit to the Auger coefficient inputs.
3. The bulk SRH, radiative, and J_{0s} components determined from the fit were subtracted from τ_{eff}^{-1}, and C_{amb} was reassessed from the slope of the corrected $\tau_{eff}^{-1}(p_0 + n_0 + \Delta n)^{-1}$ vs Δn over the original range of $5 \times 10^{15}\,\mathrm{cm^{-3}} \leq \Delta n \leq 1.5 \times 10^{16}\,\mathrm{cm^{-3}}$. By fitting in this range, where Auger recombination is dominant, we limit the sensitivity of the extracted value of C_{amb} to τ_{SRH}.
4. C_n and C_p were recalculated from (16) using the new value for C_{amb} and the intercepts of the fits to the corrected data for Samples #2 and #3.
5. The procedure was iterated to achieve self-consistency of C_{amb} and C_n/C_p.

For Samples #2 and #3, the additional constraint was imposed that the product of B_{total} and the sample thickness W be the same for both samples, as required for self-consistency with (16). Note that although strictly only the surface and not the radiative component should vary with thickness in this manner, in this case approximation introduces negligible error, since (i) the thickness difference between the samples is very small (1.4 %), (ii) the radiative component, after accounting for photon recycling, is expected to account for only a small fraction (~7 %) of B_{total}, and (iii) the radiative component will also decrease slightly with increasing thickness due to increasing photon recycling [29].

We note that in the applied correction procedure, the value of C_{amb} is relatively insensitive to the share of recombination attributed to bulk SRH or to B_{total} in the fit, however C_n/C_p is relatively sensitive to this split, and therefore significantly greater uncertainty should be attached to the latter value. By the same token, since C_n is several times larger then C_p, any uncertainty in C_n/C_p translates into significantly larger relative uncertainty in C_p than in C_n.

References

[1] A. Richter, S.W. Glunz, F. Werner, J. Schmidt, A. Cuevas, Improved quantitative description of Auger recombination in crystalline silicon, Phys. Rev. B 86 (2012).
[2] M.J. Kerr, A. Cuevas, General parameterization of Auger recombination in crystalline silicon, J. Appl. Phys. 91 (4) (2002) 2473–2480.
[3] R. Häcker, A. Hangleiter, Intrinsic upper limits of the carrier lifetime in silicon, J. Appl. Phys. 75 (11) (1994) 7570–7572.

[4] P.P. Altermatt, J. Schmidt, G. Heiser, A.G. Aberle, Assessment and parameterisation of Coulomb-enhanced Auger recombination coefficients in lowly injected crystalline silicon, J. Appl. Phys. 82 (10) (1997) 4938–4944.

[5] G. Lasher, F. Stern, Spontaneous and stimulated recombination radiation in semiconductors, Phys. Rev. 133 (1964) A553–A563.

[6] P. Würfel, The chemical potential of radiation, J. Phys. C: Solid State Phys. 15 (18) (1982) 3967–3985.

[7] T. Trupke, M.A. Green, P. Würfel, P.P. Altermatt, A. Wang, J. Zhao, R. Corkish, Temperature dependence of the radiative recombination coefficient of intrinsic crystalline silicon, J. Appl. Phys. 94 (8) (2003) 4930–4937.

[8] P.P. Altermatt, F. Geelhaar, T. Trupke, X. Dai, A. Neisser, E. Daub, Injection dependence of spontaneous radiative recombination in c-Si: experiment, theoretical analysis, and simulation, in: Proceedings of the 5th International Conference on Numerical Simulation of Optoelectronic Devices, 2005, NUSOD '05, 2005, pp. 47–48.

[9] P. Altermatt, F. Geelhaar, T. Trupke, X. Dai, A. Neisser, E. Daub, Injection dependence of spontaneous radiative recombination in crystalline silicon: Experimental verification and theoretical analysis, Appl. Phys. Lett. 88 (26) (2006) 261901.

[10] H.T. Nguyen, S.C. Baker-Finch, D. Macdonald, Temperature dependence of the radiative recombination coefficient in crystalline silicon from spectral photoluminescence, Appl. Phys. Lett. 104 (11) (2014) 112105.

[11] E. Yablonovitch, T. Gmitter, Auger recombination in silicon at low carrier densities, Appl. Phys. Lett. 49 (10) (1986) 587–589.

[12] J. Schmidt, M. Kerr, P.P. Altermatt, Coulomb-enhanced Auger recombination in crystalline silicon at intermediate and high injection densities, J. Appl. Phys. 88 (3) (2000) 1494–1497.

[13] P.P. Altermatt, J. Schmidt, M. Kerr, G. Heiser, A.G. Aberle, Exciton-enhanced Auger recombination in crystalline silicon under intermediate and high injection conditions, in: Proceedings of the 16th European Photovoltaic Solar Energy Conference, 2000, pp. 243–246.

[14] S.W. Glunz, D. Biro, S. Rein, W. Warta, Field-effect passivation of the SiO_2–Si interface, J. Appl. Phys. 86 (1) (1999) 683–691.

[15] Y. Wan, K.R. McIntosh, A.F. Thomson, Characterisation and optimisation of PECVD SiN_x as an antireflection coating and passivation layer for silicon solar cells, AIP Adv. 3 (3) (2013) 032113.

[16] B.A. Veith-Wolf, J. Schmidt, Unexpectedly high minority-carrier lifetimes exceeding 20 ms measured on 1.4-Ω cm n-type silicon wafers, Phys. Status Solidi RRL 11 (11) (2017) 1700235.

[17] N.E. Grant, T. Niewelt, N.R. Wilson, E.C. Wheeler-Jones, J. Bullock, M. Al-Amin, M.C. Schubert, A.C. van Veen, A. Javey, J.D. Murphy, Superacid-treated silicon surfaces: extending the limit of carrier lifetime for photovoltaic applications, IEEE J. Photovolt. 7 (6) (2017) 1574–1583.

[18] T. Niewelt, A. Richter, T.C. Kho, N.E. Grant, R.S. Bonilla, B. Steinhauser, J.-I. Polzin, F. Feldmann, M. Hermle, J.D. Murphy, S.P. Phang, W. Kwapil, M.C. Schubert, Taking monocrystalline silicon to the ultimate lifetime limit, Sol. Energy Mater. Sol. Cells 185 (2018) 252–259.

[19] B.A. Veith-Wolf, S. Schäfer, R. Brendel, J. Schmidt, Reassessment of intrinsic lifetime limit in n-type crystalline silicon and implication on maximum solar cell efficiency, Sol. Energy Mater. Sol. Cells 186 (2018) 194–199.

[20] B. Steinhauser, J.-I. Polzin, F. Feldmann, M. Hermle, S.W. Glunz, Excellent surface passivation quality on crystalline silicon using industrial-scale direct-plasma TOPCon deposition technology, Solar RRL 2 (7) (2018) 1800068.

[21] T.C. Kho, K. Fong, K. McIntosh, E. Franklin, N. Grant, M. Stocks, S.P. Phang, Y. Wan, E.-C. Wang, K. Vora, Z. Ngwe, A. Blakers, Exceptional silicon surface passivation by an ONO dielectric stack, Sol. Energy Mater. Sol. Cells 189 (2019) 245–253.

[22] B. Veith, T. Ohrdes, F. Werner, R. Brendel, P.P. Altermatt, N.-P. Harder, J. Schmidt, Injection dependence of the effective lifetime of n-type Si passivated by Al_2O_3: An edge effect? Sol. Energy Mater. Sol. Cells 120, Part A (2014) 436–440.

[23] N.E. Grant, V.P. Markevich, J. Mullins, A.R. Peaker, F. Rougieux, D. Macdonald, Thermal activation and deactivation of grown-in defects limiting the lifetime of float-zone silicon, Phys. Status Solidi RRL 10 (6) (2016) 443–447.

[24] N.E. Grant, V.P. Markevich, J. Mullins, A.R. Peaker, F. Rougieux, D. Macdonald, J.D. Murphy, Permanent annihilation of thermally activated defects which limit the lifetime of float-zone silicon, Phys. Status Solidi a 213 (11) (2016) 2844–2849.

[25] T. Niewelt, B. Steinhauser, A. Richter, B. Veith-Wolf, A. Fell, N.E. Grant, L.E. Black, J.D. Murphy, M.C. Schubert, S.W. Glunz, Reassessment of the intrinsic bulk recombination in crystalline silicon, 2021 in preparation.

[26] R.A. Sinton, R.M. Swanson, Recombination in highly injected silicon, IEEE Trans. Electron Devices 34 (6) (1987) 1380–1389.

[27] D.E. Kane, R.M. Swanson, Measurement of the emitter saturation current by a contactless photoconductivity decay method, in: Conf. Rec. 18th IEEE Photovoltaic Specialists Conf., Las Vegas, USA, 1985, pp. 578–583.

[28] L.E. Black, D.H. Macdonald, Accounting for the dependence of coil sensitivity on sample thickness and lift-off in inductively coupled photoconductance measurements, IEEE J. Photovolt. 9 (6) (2019) 1563–1574.

[29] A. Fell, T. Niewelt, B. Steinhauser, F.D. Heinz, M.C. Schubert, S.W. Glunz, Radiative recombination in silicon photovoltaics: Modeling the influence of charge carrier densities and photon recycling, Sol. Energy Mater. Sol. Cells 230 (2021) 111198.

[30] K.R. McIntosh, L.E. Black, On effective surface recombination parameters, J. Appl. Phys. 116 (1) (2014).

[31] H. Schlangenotto, H. Maeder, W. Gerlach, Temperature dependence of the radiative recombination coefficient in silicon, Phys. Status Solidi a 21 (1) (1974) 357–367.

[32] A. Hangleiter, R. Häcker, Enhancement of band-to-band Auger recombination by electron-hole correlations, Phys. Rev. Lett. 65 (1990) 215–218.

[33] L.E. Black, W.M.M.E. Kessels, PO_x/Al_2O_3 stacks: Highly effective surface passivation of crystalline silicon with a large positive fixed charge, Appl. Phys. Lett. 112 (20) (2018) 201603.

[34] L.E. Black, W.M.M.E. Kessels, Investigation of crystalline silicon surface passivation by positively charged PO_x/Al_2O_3 stacks, Sol. Energy Mater. Sol. Cells 185 (2018) 385–391.

[35] L.E. Black, M. Ernst, R. Theeuwes, J. Melskens, D. Macdonald, W.M.M.E. Kessels, Self-aligned local contact opening and n+ diffusion by single-step laser doping from PO_x/Al_2O_3 passivation stacks, Sol. Energy Mater. Sol. Cells 217 (2020) 110717.

[36] J. Melskens, R.J. Theeuwes, L.E. Black, W.-J.H. Berghuis, B. Macco, P.C.P. Bronsveld, W.M.M. Kessels, Excellent passivation of n-type silicon surfaces enabled by pulsed-flow plasma-enhanced chemical vapor deposition of phosphorus oxide capped by aluminum oxide, Phys. Status Solidi RRL 15 (1) (2021) 2000399.

[37] G. Dingemans, M.C.M.v.d. Sanden, W.M.M. Kessels, Influence of the deposition temperature on the c-Si surface passivation by Al_2O_3 films synthesized by ALD and PECVD, Electrochem. Solid State Lett. 13 (3) (2010) H76–H79.

[38] D.B.M. Klaassen, A unified mobility model for device simulation—I. Model equations and concentration dependence, Solid-State Electron. 35 (7) (1992) 953–959.

[39] D.B.M. Klaassen, A unified mobility model for device simulation—II. Temperature dependence of carrier mobility and lifetime, Solid-State Electron. 35 (7) (1992) 961–967.

[40] F. Dannhäuser, Die abhängigkeit der trägerbeweglichkeit in silizium von der konzentration der freien ladungsträger—I, Solid-State Electron. 15 (12) (1972) 1371–1375.

[41] J. Krausse, Die abhängigkeit der trägerbeweglichkeit in silizium von der konzentration der freien ladungsträger—II, Solid-State Electron. 15 (12) (1972) 1377–1381.

[42] W.R. Thurber, R.L. Mattis, Y.M. Liu, J.J. Filliben, Resistivity-dopant density relationship for boron-doped silicon, J. Electrochem. Soc. 127 (10) (1980) 2291–2294.

[43] W.R. Thurber, R.L. Mattis, Y.M. Liu, J.J. Filliben, Resistivity-dopant density relationship for phosphorus-doped silicon, J. Electrochem. Soc. 127 (8) (1980) 1807–1812.

[44] H. Nagel, C. Berge, A.G. Aberle, Generalized analysis of quasi-steady-state and quasi-transient measurements of carrier lifetimes in semiconductors, J. Appl. Phys. 86 (11) (1999) 6218–6221.

[45] J. Brody, A. Rohatgi, A. Ristow, Guidelines for more accurate determination and interpretation of effective lifetime from measured quasi-steady-state photoconductance, in: Proc. 11th Workshop on Crystalline Silicon Solar Cell Materials and Processes, Estes Park, Colorado, 2001, pp. 163–167.

[46] F.E. Rougieux, P. Zheng, M. Thiboust, J. Tan, N.E. Grant, D.H. Macdonald, A. Cuevas, A contactless method for determining the carrier mobility sum in silicon wafers, IEEE J. Photovolt. 2 (1) (2012) 41–46.

[47] A. Savitzky, M.J.E. Golay, Smoothing and differentiation of data by simplified least squares procedures, Anal. Chem. 36 (8) (1964) 1627–1639.

[48] L.E. Black, T. Allen, K.R. McIntosh, A. Cuevas, Effect of boron concentration on recombination at the p-Si–Al_2O_3 interface, J. Appl. Phys. 115 (9) (2014).

[49] A. Schenk, Advanced Physical Models for Silicon Device Simulation, Springer Science & Business Media, 1998.

[50] P.P. Altermatt, Models for numerical device simulations of crystalline silicon solar cells–a review, J. Comput. Electron. 10 (3) (2011) 314.

[51] P.P. Altermatt, A. Schenk, F. Geelhaar, G. Heiser, Reassessment of the intrinsic carrier density in crystalline silicon in view of band-gap narrowing, J. Appl. Phys. 93 (3) (2003) 1598–1604.

[52] J. Dziewior, W. Schmid, Auger coefficients for highly doped and highly excited silicon, Appl. Phys. Lett. 31 (5) (1977) 346–348.

[53] J.D. Beck, R. Conradt, Auger-rekombination in Si, Solid State Commun. 13 (1) (1973) 93–95.

[54] J. del Alamo, S. Swirhun, R.M. Swanson, Simultaneous measurement of hole lifetime, hole mobility and bandgap narrowing in heavily doped n-type silicon, in: 1985 International Electron Devices Meeting, 1985, pp. 290–293.

[55] S.E. Swirhun, J.A. del Alamo, R.M. Swanson, Measurement of hole mobility in heavily doped n-type silicon, IEEE Electron Device Lett. 7 (3) (1986) 168–171.

[56] S.E. Swirhun, Y.-H. Kwark, R.M. Swanson, Measurement of electron lifetime, electron mobility and band-gap narrowing in heavily doped p-type silicon, in: 1986 International Electron Devices Meeting, 1986, pp. 24–27.

[57] J.C. Irvin, Resistivity of bulk silicon and of diffused layers in silicon, Bell Syst. Tech. J. 41 (2) (1962) 387–410.

[58] G. Masetti, M. Severi, S. Solmi, Modeling of carrier mobility against carrier concentration in arsenic-, phosphorus-, and boron-doped silicon, IEEE Trans. Electron Devices 30 (7) (1983) 764–769.

[59] T.F. Ciszek, T. Wang, T. Schuyler, A. Rohatgi, Some effects of crystal growth parameters on minority carrier lifetime in float-zoned silicon, J. Electrochem. Soc. 136 (1) (1989) 230–234.
[60] M.J. Kerr, Surface, Emitter and Bulk Recombination in Silicon and Development of Silicon Nitride Passivated Solar Cells (Ph.D. thesis), The Australian National University, 2002.
[61] E.H. Nicollian, J.R. Brews, MOS (Metal Oxide Semiconductor) Physics and Technology, John Wiley & Sons, New York, 1982.
[62] T. Hoshikawa, X. Huang, K. Hoshikawa, S. Uda, Relationship between gallium concentration and resistivity of gallium-doped Czochralski silicon crystals: investigation of a conversion curve, Japan. J. Appl. Phys. 47 (12) (2008) 8691–8695.
[63] P. Jonsson, H. Bleichner, M. Isberg, E. Nordlander, The ambipolar Auger coefficient: Measured temperature dependence in electron irradiated and highly injected n-type silicon, J. Appl. Phys. 81 (5) (1997) 2256–2262.
[64] B. Davies, R.G. Storer, Correlation function in a plasma at zero particle separation, Phys. Rev. 171 (1968) 150–151.
[65] F. Geelhar, Coulomb Correlation Effects in Silicon Devices (Ph.D. thesis), Swiss Federal Institute of Technology Zurich, 2004.
[66] V. Grivitskas, M. Willander, J. Vaitkus, The role of intercarrier scattering in excited silicon, Solid-State Electron. 27 (6) (1984) 565–572.
[67] D.H. Neuhaus, P.P. Altermatt, A.B. Sproul, R.A. Sinton, A. Schenk, A. Wang, A.G. Aberle, Method for measuring minority and majority carrier mobilities in solar cells, in: Proc. 17th European Photovoltaic Solar Energy Conf., 2001, pp. 242–245.
[68] P. Zheng, F.E. Rougieux, D. Macdonald, A. Cuevas, Measurement and parameterization of carrier mobility sum in silicon as a function of doping, temperature and injection level, IEEE J. Photovolt. 4 (2) (2014) 560–565.
[69] P. Zheng, F.E. Rougieux, D. Macdonald, A. Cuevas, Parameterization of carrier mobility sum in silicon as a function of doping, temperature and injection level: Extension to p-type silicon, in: Proc. 40th IEEE Photovoltaic Specialist Conf., 2014, pp. 0129–0134.
[70] Z. Hameiri, F. Rougieux, R. Sinton, T. Trupke, Contactless determination of the carrier mobility sum in silicon wafers using combined photoluminescence and photoconductance measurements, Appl. Phys. Lett. 104 (7) (2014) 073506.
[71] J.M. Dorkel, P. Leturcq, Carrier mobilities in silicon semi-empirically related to temperature, doping and injection level, Solid-State Electron. 24 (9) (1981) 821–825.
[72] A. Cuevas, R. Sinton, Detailed modelling of silicon solar cells, in: Proc. 23rd European Photovoltaic Solar Energy Conf., 2008 pp. 315–319.
[73] A. Cuevas, Modelling silicon characterisation, Energy Procedia 8 (2011) 94–99.
[74] T. Trupke, R.A. Bardos, M.D. Abbott, Self-consistent calibration of photoluminescence and photoconductance lifetime measurements, Appl. Phys. Lett. 87 (18) (2005) 184102.
[75] J.A. Giesecke, T. Niewelt, M. Rüdiger, M. Rauer, M.C. Schubert, W. Warta, Broad range injection-dependent minority carrier lifetime from photoluminescence, Sol. Energy Mater. Sol. Cells 102 (2012) 220–224.
[76] R. Couderc, M. Amara, M. Lemiti, Reassessment of the intrinsic carrier density temperature dependence in crystalline silicon, J. Appl. Phys. 115 (9) (2014) 093705.
[77] A. Kimmerle, M. Momtazur Rahman, S. Werner, S. Mack, A. Wolf, A. Richter, H. Haug, Precise parameterization of the recombination velocity at passivated phosphorus doped surfaces, J. Appl. Phys. 119 (2) (2016) 025706.
[78] A. Wolf, J. Egle, S. Mack, H. Höffler, D. Herrmann, S. Lohmüller, J. Horzel, A. Fell, Revised parametrization of the recombination velocity at SiO_2/SiN_x-passivated phosphorus-diffused surfaces, Sol. Energy Mater. Sol. Cells 231 (2021) 111292.
[79] D. Yan, A. Cuevas, Empirical determination of the energy band gap narrowing in highly doped n+ silicon, J. Appl. Phys. 114 (4) (2013).
[80] D. Yan, A. Cuevas, Empirical determination of the energy band gap narrowing in p+ silicon heavily doped with boron, J. Appl. Phys. 116 (19) (2014) 194505.